Climate Dynamics (2026) 64:112
https://doi.org/10.1007/s00382-026-08098-z

ORIGINAL ARTICLE

Influence of persistent soil temperature and soil moisture anomalies on land surface fluxes in China

Yaoming Song[1,2] · Wei Gu[3] · Anning Huang[4] · Taotao Zhang[1,2] · Haishan Chen[1,2]

Received: 22 September 2025 / Accepted: 29 January 2026

Abstract
Radiation, sensible and latent heat fluxes are critical in the influence of antecedent and simultaneous soil moisture (SM) and soil temperature (ST) on atmosphere. However, how the persistence of antecedent SM/ST anomalies influences current land surface fluxes is not yet fully understood. Based on reanalysis dataset, observations and numerical experiments, using the concept of simply connected space, this study investigates the maximum lead time at which antecedent SM/ST remain significantly correlated with current surface-layer SM/ST (MLTSM/MLTST), and the intensity of antecedent SM/ST's influence on current surface fluxes. Results show that the SM/ST and land surface flux data from ERA5-Land exhibits closer temporal agreement with observations than those from GLDAS, MERRA-2 and NCEP. In spring and summer, the surface-layer ST correlates significantly with antecedent ST over a longer lead time than that in autumn and winter, particularly in MLTST in the area (33° N–42° N, 105° E–120° E). In this area, the impact of antecedent ST on surface fluxes is significantly pronounced. The surface-layer SM correlates significantly with antecedent SM over a longer lead time in winter and spring than that in summer and autumn, and the influence of antecedent SM on surface fluxes varies across areas and seasons. Moreover, antecedent signals with a long lead time and strong association with surface-layer ST and SM predominantly originate from deep soil layers. The conclusions from ERA5-Land demonstrate closer agreement with the simulations. The east-low–west-high spatial pattern of MLTSM is also partially captured in the simulations.

Keywords Soil temperature · Soil moisture · Persistence · Land surface fluxes

1 Introduction

As an important component of climate system, land surface plays a non-negligible role in climate change. The nature of climate prediction depends mainly on the lead-lag relationships between the variables in the atmosphere, ocean and land, and the lead-lag relationships are attributed to the persistence of the anomalies of the variables. The variable anomalies in the atmosphere can persist for about ten days due to the chaotic nature (Lorenz 1969; Mariotti et al. 2018; Krishnamurthy 2019), and the slowly varying variables in the land and ocean provide basis for climate prediction for long time range.

Soil moisture (SM) is a key factor in land–atmosphere interactions, the anomalies of SM can be maintained in the soil at monthly to seasonal scales (Koster and Suarez 2001; Dirmeyer et al. 2009). In mid-latitudes, tropics, and subtropics, the overall impact of SM on warm season terrestrial climate is similar to that of sea surface temperature (Orth and Seneviratne 2017). However, the effect of SM on climate is

✉ Yaoming Song
songym@nuist.edu.cn

1 State Key Laboratory of Climate System Prediction and Risk Management/Key Laboratory of Meteorological Disaster, Ministry of Education/Collaborative Innovation Center On Forecast and Evaluation of Meteorological Disasters, Nanjing University of Information Science and Technology, Nanjing 210044, China

2 School of Atmospheric Sciences, Nanjing University of Information Science and Technology, Nanjing, Jiangsu, China

3 Laboratory for Climate Studies, National Climate Center, China Meteorological Administration, Beijing, China

4 School of Atmospheric Sciences, Nanjing University, Nanjing, China

Published online: 19 February 2026

largely independent of the effect of sea surface temperature on climate (Orth and Seneviratne 2017). Antecedent SM anomalies can provide important information for subseasonal and seasonal weather forecasts (Orth and Seneviratne 2017). SM is an important precursor signal for forecasting and predictability in addition to sea surface temperature (Seneviratne et al. 2010; Dorigo et al. 2017; Santanello et al. 2018). Numerous studies have confirmed the important role of SM in subsequent precipitation (Zhan and Lin 2011; Zhong et al 2018; Zhang and Zuo 2011; Meng et al. 2014; Liu et al. 2017; Beljaars et al. 1996; Gao et al. 2014; Dong et al. 2023; Yoon et al. 2015), air temperature and heat wave (Alfaro et al. 2006; Fischer et al. 2007; Weisheimer et al. 2011; Quesada et al. 2012; Miralles et al. 2014; Prodhomme et al. 2016), dust emission (Kim and Choi 2015), and wildfire prediction (Krueger et al. 2016).

Soil temperature (ST) is another key factor in land–atmosphere interactions, and is a critical indicator of soil heat storage. The persistence of ST anomalies (ST memory) can affect the subsequent weather and climate. The anomalies of ST can persist for several months (Yang and Zhang 2016; Zhao et al. 2018; Liu et al. 2020; Zhang et al. 2021; Song et al. 2022a). The ST in winter may affect the precipitation in the following flood season (Tang et al. 1987). Based on observation and reanalysis data, the winter soil on the Tibetan Plateau can remember surface temperature anomalies and lead to surface temperature anomalies in the next summer (Lin et al. 2022). Moreover, some studies have confirmed the important effect of spring ST on summer precipitation. The three long-term Atmospheric Model Intercomparison Project-type experiments showed that the ST in late spring is an important factor affecting the precipitation in summer (Mahanama et al. 2008). Both observation analysis and numerical simulations suggested that the precipitation in summer in North America and East Asia is closely related to the upstream ST anomalies in spring (Xue et al. 2012, 2018). The spring ST anomalies in West Asia can lead to the anomalies of precipitation and air temperature in Northeast China in June through diabatic heating (Yang et al. 2021). There are also some studies on the impact of the ST in other months and seasons on subsequent air temperature and precipitation. The ST anomalies in May over Northwest China can modulate the East Asian summer monsoon and then change the precipitation in summer (Wang et al. 2013). Using RegCM4 model, antecedent ST has a strong impact on air temperature at the monthly and seasonal scales in China (Liu et al. 2015). Based on the atmospheric model ECHAME5 coupled with the Common land model, the ST in May from the middle and lower reaches of the Yangtze River to North China has important impacts on the precipitation in eastern China through adjusting atmospheric circulation (Zhou et al. 2020). Observation analysis showed that the severe floods correspond to high antecedent ST in Yangtze-Huaihe River basin, while the severe drought corresponds to low antecedent ST in the south of Yangtze River (Ma 1995). ST also plays a crucial role in the monthly lead-lag correlation of air temperature at 2 m in the middle and lower reaches of the Yangtze River Basin (Song et al. 2023). Additionally, some studies revealed the role of antecedent ST in the extreme event (Gómez et al. 2016).

Climate prediction relies on the atmospheric response to the anomalies of the variables in the land and ocean, and on the persistence of the anomalies of the variables. The sensitivity of current atmospheric state to antecedent land and ocean variables was primarily governed by the anomalies in current radiation fluxes, sensible heat fluxes (SH) and latent heat fluxes (LH) caused by current land or ocean variable anomalies which are affected by the persistence of the antecedent land or ocean variable anomalies. Therefore, the effect of antecedent land surface variable anomalies on local or non-local precipitation or air temperature is attributed to three key processes. One process is the persistence of antecedent land surface variable anomalies in the soil, the second is the influence of the persistent variable anomalies on current local radiation, sensible and latent fluxes, and the third is the impact of these current local surface fluxes on local and remote atmospheric conditions. Although many studies have confirmed the impact of antecedent SM and ST on subsequent climate conditions, a clear and in-depth understanding of how antecedent SM and ST affect current land surface fluxes remains limited. Elucidating this relationship is essential, as it determines the potential influence of antecedent SM and ST on subsequent atmospheric conditions. Moreover, the ST and SM observation data is very limited, and there are numerous missing values in these data. Therefore, reanalysis data is utilized as a substitute for the observations. However, there is a lack of evaluation of whether the ST and SM in the reanalysis data can reproduce the persistence characteristics of ST and SM anomalies found in the observed data. To address the above issues, this study focuses on three key questions: (1) Which reanalysis data can better reproduce the persistent characteristics of ST and SM anomalies in the observed data? (2) What is the maximum lead time of antecedent SM/ST significantly related to current SM/ST? (3) To what extent do antecedent ST and SM influence current surface fluxes by modifying current ST and SM?

2 Data, model and methodology

2.1 Data

The following reanalysis datasets were utilized: ERA5-Land, NCEP, MERRA-2 and GLDAS-CLSM. The variables from ERA5-Land (Hersbach et al. 2018; Herbach et al. 2020) include monthly surface latent heat flux (LH), sensible heat flux (SH), emitted thermal radiation (emittedLW), downward thermal radiation, net solar radiation, downward solar radiation, skin temperature (SKT), precipitation, evapotranspiration, air temperature, ST and SM in four soil layers. The four soil layers are 0 to 0.07 m, 0.07 to 0.28 m, 0.28 to 1.00 m and 1.00 to 2.89 m, respectively. The above data spans from 1979 to 2022, and spatial resolution is $0.1° \times 0.1°$. More information on the above data can be obtained from the website: http://apps.ecmwf.int/data-catalogues/era5.

GLDAS-CLSM dataset (Gelaro et al. 2017) also is utilized, and the variables include the ST and SM in 6 soil layers (0–0.10 m, 0.10–0.29 m, 0.29–0.68 m, 0.68–1.44 m, 1.44–2.95 m, and 2.95–12.95 m) from 1979 to 2022. GLDAS is the land surface data product that optimally combines land surface process modeling with multi-source observational data assimilation. The GLDAS-CLSM specifically employs the Catchment Land surface model. Detailed documentation is available at https://ldas.gsfc.nasa.gov/gldas.

NCEP-DOE Reanalysis II (R-2) represents an enhanced version of the original NCEP Reanalysis I (R-1), incorporating corrected systematic errors and updated parameterizations of key physical processes. It provides gridded data fields assimilated from multiple observational sources, including surface instruments, radiosondes, aircraft reports, and satellite measurements. For this study, we utilized monthly mean ST and SM data spanning the period from January 1979 to December 2022. Soil layers were defined as 0–0.1 m (surface layer) and 0.1–2 m (subsurface layer). The detailed documentation of the dataset can be found at https://psl.noaa.gov/data/gridded/data.ncep.reanalysis2.html.

MERRA-2 (Modern-Era Retrospective analysis for Research and Applications, Version 2) represents NASA's global atmospheric reanalysis product for the satellite era. Developed by the Global Modeling and Assimilation Office, this dataset is generated using the Goddard Earth Observing System Model with advanced data assimilation techniques. For this study, we utilized monthly mean ST and SM data spanning the period from January 1979 to December 2022. SM is represented by two soil layers (0–0.05 m and 0.1–1 m), while ST were calculated at six soil depths (0.0988, 0.1952, 0.3859, 0.7626, 1.5071 and 10 m). The detailed can be found at https://disc.gsfc.nasa.gov/datasets/M2T1NXLND_5.12.4/summary?keywords=MERRA2

The SM and ST observations are provided by the China Meteorological Administration. The dataset comprises monthly average ST in the 7 soil layers of 0.05, 0.10, 0.20, 0.40, 0.80, 1.60 and 3.20 m at 2479 sites from 1960 to 2013, the 10-day interval SM at the soil depths of 0.1 m and 0.2 m at 778 sites from 1991 to 2010, and the field water-holding capacity at 178 sites from 1981 to 1998. The monthly temperature at 2 m (T2m) and precipitation observation data for 2023 and 2024 are available from the China Meteorological Administration.

2.2 Model

To cross-validate the conclusions derived from reanalysis data, the Weather Research and Forecasting (WRF) model 4.3 (Skamarock et al. 2008) was employed to analyze the persistence of ST and SM anomalies in January and July under land–atmosphere coupling conditions and their influence on subsequent surface fluxes. Centered at (35°N, 100°E), the simulation domain comprises 80 grid points in the west–east direction and 50 in the south-north direction, with a horizontal grid spacing of 100 km. NCEP-FNL data were used to provide initial and boundary conditions. The simulation period spans from 2023 to 2024, which is a recent time frame chosen to facilitate more accurate evaluation of WRF model performance against observational data.

Two control experiments, designated as CTL-WRF-JAN and CTL-WRF-JUL, were carried out covering the periods from January 1 to December 31, 2023, and July 1, 2023, to June 30, 2024, respectively. Additionally, four sensitivity experiments, labeled JAN-ST, JAN-SM, JUL-ST, and JUL-SM, were initiated on January 2 and July 2, correspondingly. The initial conditions for the four sensitivity experiments were from the atmospheric and soil conditions simulated by the control experiments, with the incorporation of ST or SM anomalies. These anomalies were defined based on the standard deviation of ERA5-Land ST and SM data for January and July over the period 1979–2023.

The relationships between initial ST/SM anomalies and subsequent ST/SM anomalies of the first soil layer were obtained using the concept of simply connected space (Methodology section). Here, the simply connected space comprises spatiotemporal locations at which the ST/SM anomalies exhibit the same sign (positive or negative) as the initial ST/SM anomalies. In these simulations, the anomaly of a variable is defined as the difference in the variable between the sensitivity and the control experiment. The relationships between initial ST/SM anomalies and subsequent surface flux anomalies were obtained in the same approach.

2.3 Methodology

The observational data (OBS) from 2397 sites for ST and 160 sites for SM were utilized, following the exclusion of sites with excessive missing values. The reanalysis ST and SM data were spatially interpolated to the locations of the observational sites. The Pearson correlation coefficients between the observed SM and the reanalysis SM in the shallow soil were calculated in 12 calendar months of the year. The number of the months with statistically significant ($p<0.05$) correlation coefficients between the observed SM/ST and the reanalysis SM/ST in the shallow soil in a calendar year is shown in Fig. 1. And the ERA5-Land and MERRA-2 SM data can better reproduce the interannual variations of observed SM than the other two reanalysis SM data in the region (30° N–40° N, 100° E–120° E) (Fig. 1). According to Fig. 1a, b, the ERA5-Land and MERRA-2 SM data at the sites exhibiting statistically significant ($p<0.05$) correlation coefficients in more than 9 months of the year were utilized for subsequent analysis, and the numbers of the selected sites are 19 and 12, respectively (Fig. 2b and d). For ST, we applied the same selection method, and the numbers of the selected sites are 1692 for ERA5-Land and 1706 for MERRA-2 (Fig. 2a and c).

Based on the results in Sect. 3.3, the linear correlations between ST/SM and surface fluxes show similar monthly variations across soil layers, particularly with ST/SM in the first layer, which exhibits the strongest correlations (Fig. 3). Consequently, subsequent analysis of the influence of SM and ST on concurrent surface fluxes focused on the SM and ST of the first soil layer. Moreover, based on the results in Sect. 3.2 (Fig. 4), antecedent ST and SM can affect current surface fluxes through modifying current surface-layer ST and SM.

The relationship between antecedent ST and current ST is determined primarily based on the concept of simply connected space, with encompasses the following two aspects: (i) the spatial continuity of anomaly signal propagation (as illustrated in Fig. 5), and (ii) the statistical significance of their correlations. Based on the first criterion, when there a significant signal linkage between current ST and ST at lead time n, the following condition must be satisfied for a significant signal linkage between current ST and ST at lead time n+1:

Among the four soil layers: (a) those showing statistically significant correlations ($p<0.01$) between current ST and ST at lead time n, and (b) those showing significant correlations ($p<0.01$) between current ST and ST at lead time $n+1$, must demonstrate either spatial overlap or adjacency (at least one common or neighboring soil layer).

The existence of a significant relationship between current ST in the first soil layer and antecedent ST is determined by whether the spatiotemporal location of the antecedent ST lies within the simply connected space bounded by the blue lines in Fig. 5. Similarly, a significant relationship between antecedent SM and current SM was obtained in the same approach.

Using the above method, the relationship between antecedent SM and current SM was also obtained. Moreover, we can obtain the maximum lead time of antecedent SM/ST that is closely related to current SM/ST of the first soil layer (MLTSM/MLTST) (Fig. 5). MLTSM and MLTST determine the maximum lead time during which antecedent SM/ST can affect current surface fluxes by modifying current SM/ST.

The effect of antecedent ST/SM on subsequent surface fluxes (ASTFlux/ASMFlux) was analyzed using two-legged index (Dirmeyer 2011; Dimeyer et al. 2014). The first leg is

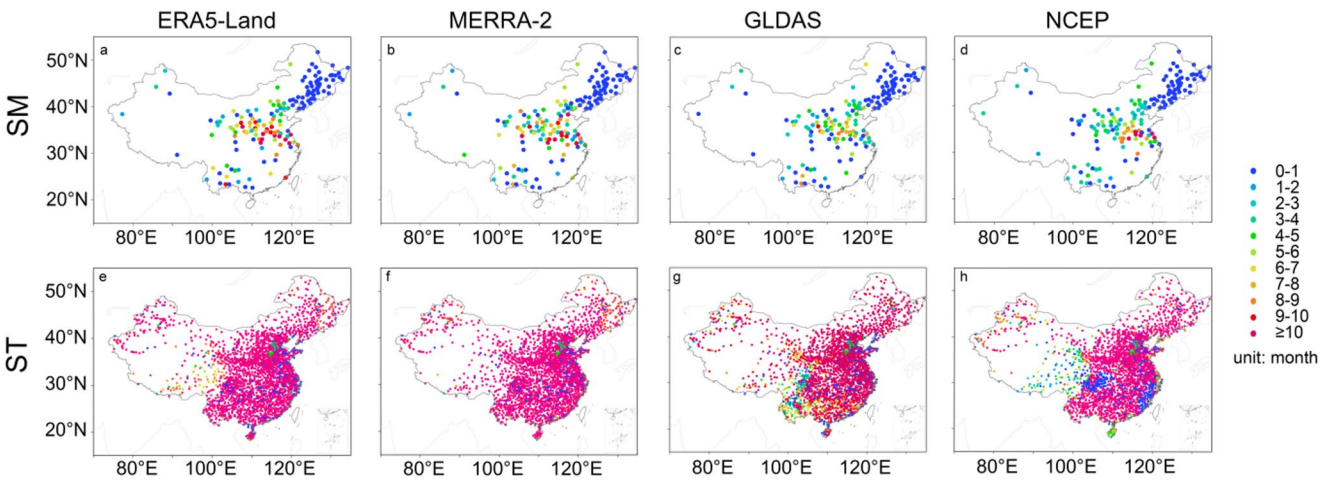

Fig. 1 The number of the months with statistically significant ($p<0.05$) correlation coefficients between the observed SM/ST and the reanalysis SM/ST in the shallow soil in a calendar year. The first, second, third and fourth columns correspond to ERA5-Land, MERRA-2, GLDAS and NCEP, respectively. The first row corresponds to SM, and the second row to ST

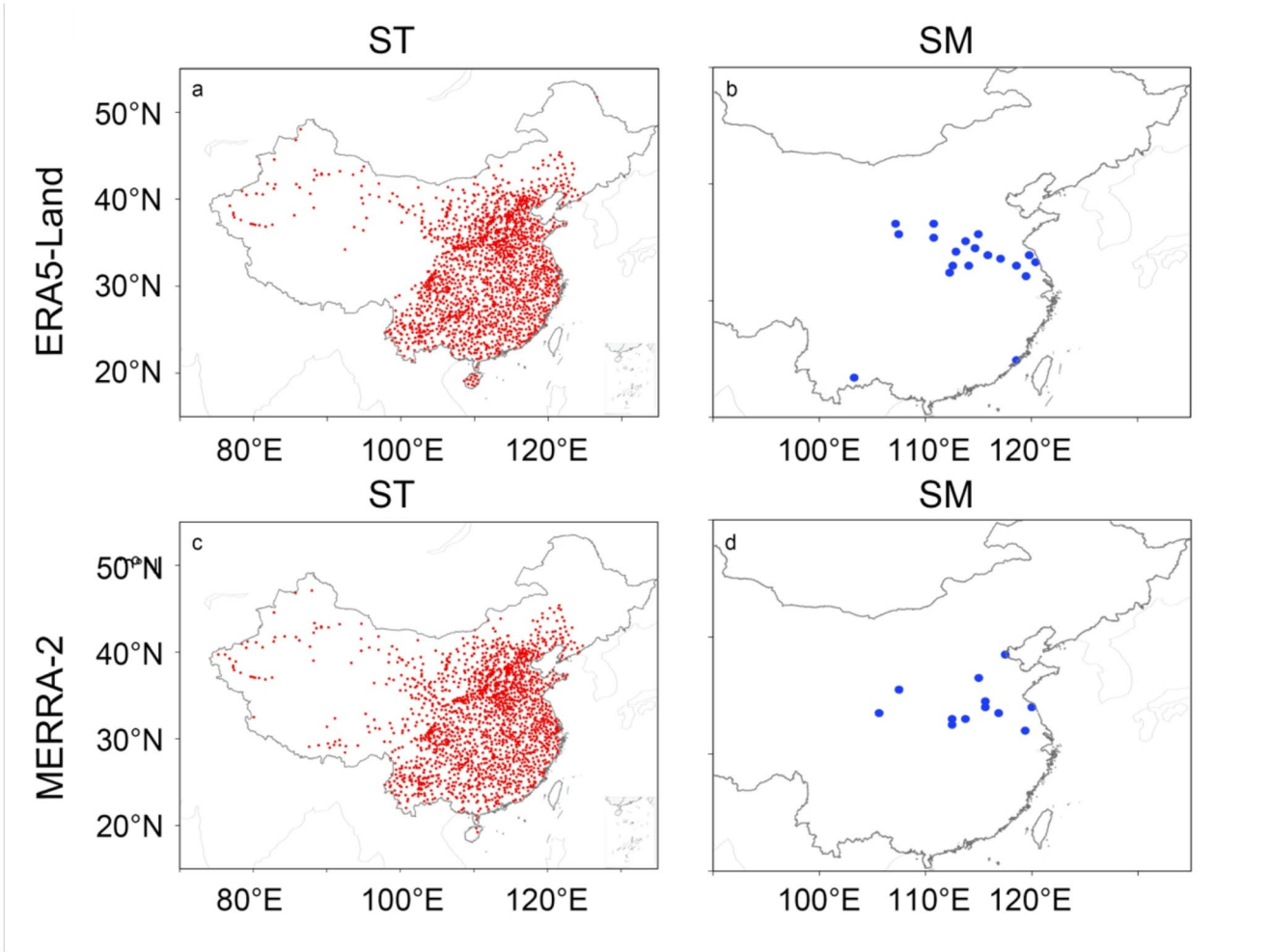

Fig. 2 The spatial distributions of the ERA5/MERRA-2 spatial grids where ST and SM data are used in the following study. **a** and **c** show the grids where the correlation coefficients between the observed SKT and the ERA5 SKT are statistically significant at the 0.05 significance level for all 12 calendar months. **b** and **d** show the grids where the correlation coefficients between the observed SM and the ERA5 SM are statistically significant at the 0.05 significance level in more than 9 months of the year

the effect of antecedent ST/SM across different soil layers on current ST/SM in the first soil layer, the second leg is the effect of current ST/SM in the first soil layer on current surface fluxes. The effect of antecedent ST/SM on surface fluxes by modifying the ST/SM in the first soil layer can be derived as follows:

Construct linear equations corresponding to ($Flux$, $SS2$) and ($SS1$, $SS2$), respectively:

$$Flux = b\ SS2 + c \tag{1}$$

$$SS2 = d\ SS1 + e \tag{2}$$

$$\rho(SS2, Flux) = b\frac{\sigma(Flux)}{\sigma(SS2)} \tag{3}$$

$$\rho(SS1, SS2) = d\frac{\sigma(SS2)}{\sigma(SS1)} \tag{4}$$

$$\begin{aligned}\frac{dFlux(SS2)}{dSS1} &= \frac{dFlux}{dSS2}\frac{dSS2}{dSS1} = b \cdot d \\ &= \left[\rho(SS2, Flux)\frac{\sigma(Flux)}{\sigma(SS2)}\right]\left[\rho(SS1, SS2)\frac{\sigma(SS2)}{\sigma(SS1)}\right] \\ &= \rho(SS2, Flux)\rho(SS1, SS2)\frac{\sigma(Flux)}{\sigma(SS1)}\end{aligned} \tag{5}$$

$$\begin{aligned}I_{SS1-SS2-Flux} &= \left[\frac{dFlux(SS2)}{dSS1}\sigma(SS1)\right]/\sigma(Flux) \\ &= \rho(SS2, Flux)\rho(SS1, SS2)\end{aligned} \tag{6}$$

where $SS1$ and $SS2$ represent antecedent ST/SM across different soil layers and current ST/SM in the first soil layer, respectively. $Flux$ is current surface fluxes. $\sigma(SS1)$, $\sigma(SS2)$ and $\sigma(Flux)$ signify the standard deviation of the variable $SS1$, $SS2$ and $Flux$, respectively.$\rho(SS1, SS2)$

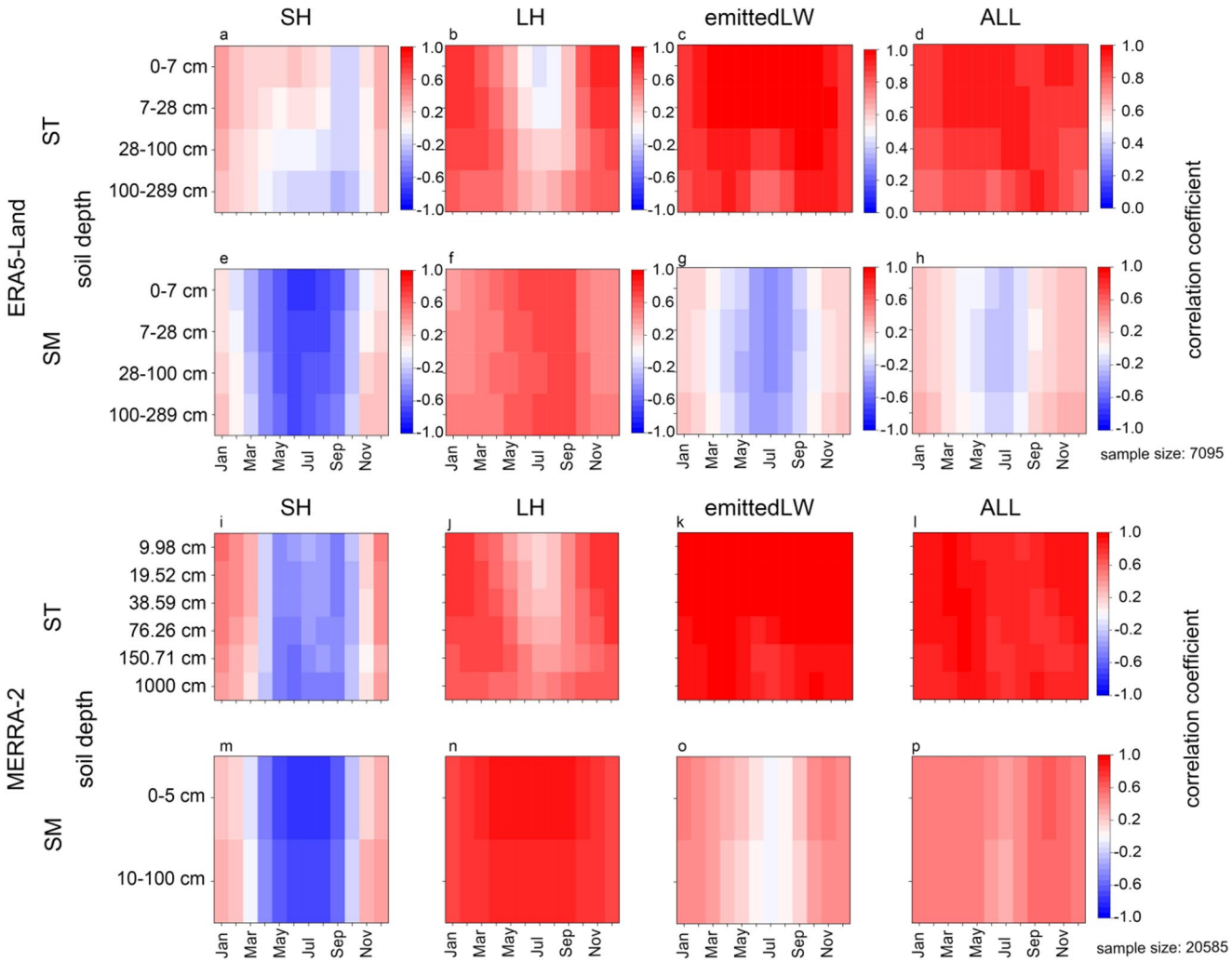

Fig. 3 Correlation coefficients between ST/SM and concurrent SH as well as LH and emittedLW. The sample size from all ERA5-Land spatial grids over 44 years, and it is $(217 \times 134 \times 44)/(5 \times 5 \times 3)$, and the sample size from all MERRA-2 grids is 20,585. The first and third rows represent the correlation coefficients between ST and simultaneous SH, LH, emittedLW and ALL (the sum of SH, LH and emittedLW). The second and fourth rows represent the correlation coefficients between SM and simultaneous SH, LH, emittedLW and ALL, respectively

denotes the correlation coefficient between $SS1$ and $SS2$. $\rho(SS2, Flux)$ is the correlation coefficient between $Flux$ and $SS2$. The values of ASTFlux and ASMFlux are assigned using $I_{SS1-SS2-Flux}$. The positive $I_{SS1-SS2-Flux}$ represents the proportion of positive $Flux$ anomalies caused by positive $SS1$ anomalies relative to the total magnitude of $Flux$ anomalies, where the total magnitude is quantified by the standard deviation of $Flux$. In contrast, the negative $I_{SS1-SS2-Flux}$ represents the proportion of negative $Flux$ anomalies caused by positive $SS1$ anomalies.a,b,c and d are constants.

3 Results

3.1 The spatial distributions of MLTSM/MLTST

As detailed in the Methodology section, using the four reanalysis ST data interpolated at 2397 sites, and then the spatial grids were selected where the correlation coefficients between reanalysis and observed ST in the shallow soil layer are statistically significant at the 0.05 level. And the numbers of selected grids with statistically significant correlations are 1692 for ERA5-Land, 1706 for MERRA-2, 1157 for GLDAS, and 1103 for NCEP, respectively. Moreover, due to the scarcity of observational ST data in middle and deep soil layers, only the observed ST data from 51 sites was used in the following analysis. The MLTST derived

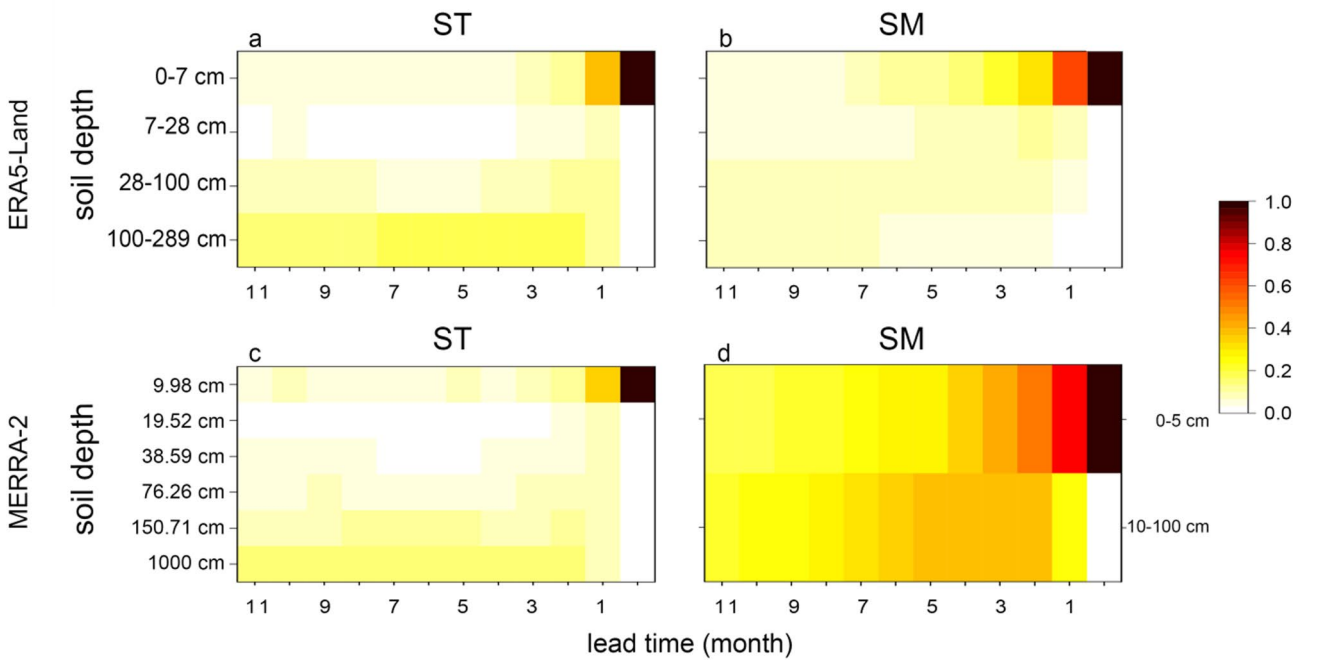

Fig. 4 The proportion of antecedent ST/SM in each soil layer that is closely related to current ST/SM of the first soil layer, relative to total samples (all spatial grids × 12 months) in ERA5-Land and MERRA-2. **a** and **b** correspond to ST and SM, respectively. Here, the antecedent ST/SM location closely related to current ST/SM is defined as satisfying two criteria: correlation coefficients passing the 99% confidence level, and its correlation strength exceeding that of all other soil depths at the same lead time

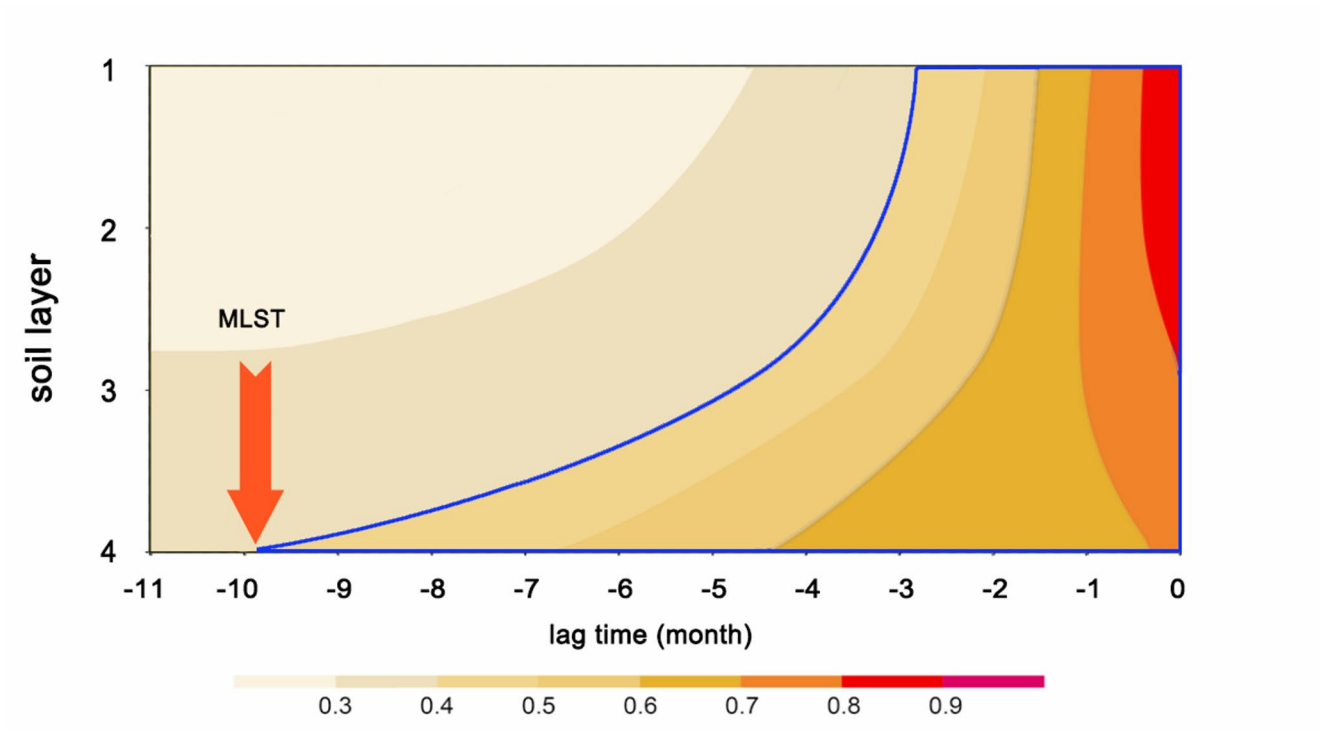

Fig. 5 The correlation coefficients between the ST in the first layer and multi-layer ST at preceding times. The correlation coefficients within the area enclosed by blue lines are statistically significant at the 99% confidence level, forming a simply connected space

from the four reanalysis ST data was evaluated. In all four seasons, in the areas south of 30°N in China, the MLTST calculated using the observed ST is primarily 0–1 month, and at several sites, it is more than 1 month (Fig. 6a, f, k and p). Except for ERA5-Land and NCEP, the MLTST calculated using MERRA-2 and GLDAS differ significantly from those calculated using OBS (Fig. 6). Moreover, in the region north of 30°N in China, the MLTST calculated using the observed ST range from 0 to 11 months. In all four seasons, the MLTST calculated using MERRA-2, GLDAS and NCEP vary significantly from those calculated using OBS. Compared with MERRA-2, GLDAS and NCEP, the MLTST calculated using ERA5-Land is similar to those calculated using OBS in terms of both spatial pattern and magnitude (Fig. 6). Therefore, the ERA5-Land ST data was used in the following analysis.

Both observation-based and ERA5-derived MLTST is higher in Area1 (Fig. S1) than that in the areas south of 33°N (Fig. 6). Area1 is defined as the area (33°N-42°N, 105°E-120°E). In the areas south of 30°N, the MLTST mainly ranges from 0 to 1 month, while it mainly ranges from 0 to 11 months in Area1. Additionally, the MLTST in spring and summer is significantly higher than that in autumn and winter. The MLTST at the two sites on the Qinghai-Tibet Plateau is relatively long, and it can reach up to 10 months in spring and winter (Fig. 6). The MLTST derived from MERRA-2 does not reproduce the spatial and seasonal characteristics seen in observation-based MLTST, specifically the south-low-north-high spatial pattern and the larger values in spring/summer compared to autumn/winter. The spatial distributions of MLTST are similar to those of the ST memory reported by Yang et al. (2016).

The MLTSM sites are located in the area spanning from 32°N to 37°N and from 105°E to 122°E (Area2) (Figs. 7 and S1). On the whole, both MERRA-2 and ERA5-Land indicate that the MLTSM decrease successively from winter to spring, spring to autumn, autumn to summer, potentially attributable to more precipitation directly affecting SM in summer. Moreover, the MLTSM is higher in the western part than in the eastern part of the Area2. In winter, the MLTSM spans from 1 to 5 months in ERA5-Land and from 3 to 11 months in MERRA-2 (Fig. 7d and h). In spring, the MLTSM varies between 0 to 5 months in ERA5-Land and from 3 to 11 months in MERRA-2 (Fig. 7a and e). In summer, the MLTSM in ERA5-Land ranges from 0 to 2 months, with the main range being from 0 to 1 month. By comparison, the MLTSM in MERRA-2 ranges from 0 to 7 months, with the main range being from 1 to 3 month. In autumn, the MLTSM in ERA5-Land ranges from 0 to 2 months, with most values lying in the 1 to 2 month period. In contrast, the MLTSM in MERRA-2 ranges from 2 to 9 months in autumn. The sites in the west have a longer MLTSM than those in the east (Fig. 7). The MLTSM spatial pattern is

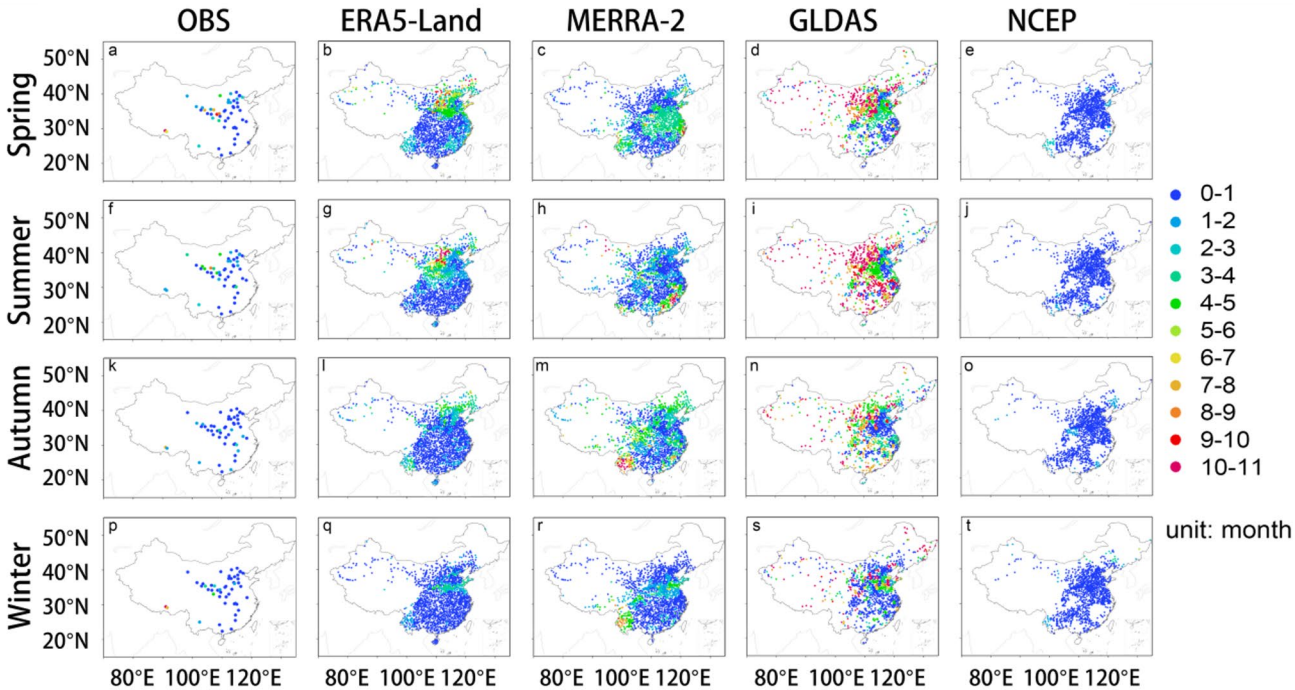

Fig. 6 The spatial distributions of the MLTST. The first, second, third and fourth columns correspond to observation (OBS), ERA5-Land, MERRA-2, GLDAS and NCEP, respectively. The first, second, third and fourth rows correspond to spring, summer, autumn and winter, respectively. The grid counts are 1692, 1706, 1157 and 1103 for ERA5-Land, MERRA-2, GLDAS and NCEP, respectively. And the site count is 51 for OBS

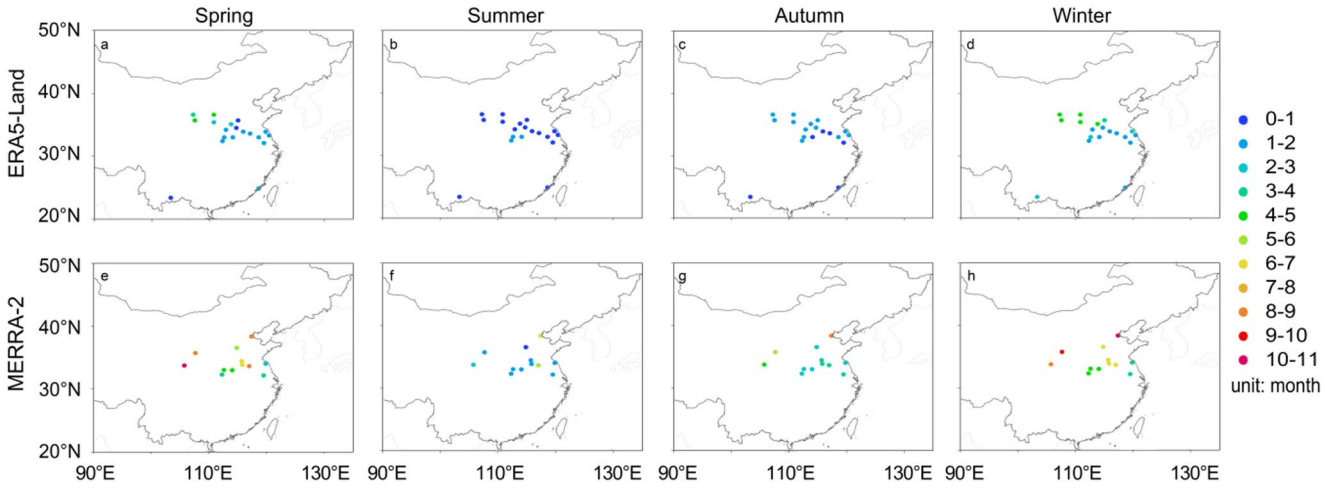

Fig. 7 The spatial distributions of the MLTSM using ERA5-Land (**a**) and MERRA-2 (**b**) SM data. The first, second, third and fourth columns correspond to spring, summer, autumn and winter, respectively. The first and second rows correspond to ERA5-Land and MERRA-2, respectively

broadly consistent with the pattern of soil moisture memory described by Li et al. (2020).

3.2 The connection of antecedent SM and ST with current SM and ST

Does antecedent ST/SM significantly influence current surface-layer ST/SM? Kumar et al. (2019) demonstrated that deeper SM anomalies appear to return to the surface when the vertical soil water potential gradient reverses its sign. Song et al. (2022a, b) revealed that antecedent deeper ST anomalies can reemerge at the surface in certain conditions. Figure 4 shows the characteristics of the soil depth of antecedent ST/SM that is statistically significantly associated with current ST/SM in the first soil layer. For ST, antecedent ST associated with current ST of the first soil layer is primarily located in middle and deep soil layers at lead times ranging from one to eleven months (Fig. 4a and c). In ERA5-Land, current SM in the first soil layer exhibits a significant association with antecedent SM in middle soil layers at lead times ranging from one to eleven months, as well as with antecedent SM in deep soil layers at lead times ranging from seven to eleven months (Fig. 4b). In contrast, in MERRA-2, current SM in the first soil layer shows a significant association with antecedent SM in all two soil layers across lead times ranging from one to eleven months (Fig. 4d). The significant correlations between antecedent deep ST/SM and current shallow ST/SM may be attributed not only to the significant correlations between antecedent atmospheric variables and current shallow ST/SM, but also to the persistence of antecedent ST/SM anomalies in the soil and their influence on current ST/SM. If the antecedent atmospheric variables determine the significant correlations between antecedent deep ST/SM and current shallow ST/SM, the correlations between antecedent shallow ST/SM should be significantly correlated with current shallow ST/SM according to the physical process of anomaly signal propagation. Therefore, the significant correlations between antecedent deep ST/SM and current shallow ST/SM shown in Fig. 4 may be attributed to the persistence of antecedent ST/SM anomalies in the soil and their influence on current ST/SM. Moreover, the statistical association between antecedent SM of the first soil layer and current SM of the first soil layer is closer than that between antecedent ST of the first soil layer and current ST of the first soil layer. Building on the evidence presented in Figs. 3 and 4, antecedent ST and SM may affect current surface fluxes through modifying current ST and SM in the first soil layer.

There is a significant connection between antecedent and current SM/ST, and there are obvious differences across different regions and seasons. So how does this connection occur? As shown in Fig. 8a and e, for MLTST exceeding 2 months, antecedent anomaly signals from two months prior associated with current ST of the first soil layer mainly originate from the middle and deep soil depth. When MLTST is not more than 2 months, antecedent anomaly signals linked to current ST are mainly from the entire soil column (Fig. 8b and f). The characteristics of antecedent anomaly signals of MLTSM differ significantly from those of MLTST. When MLTSM exceeds 2 months, antecedent signals from 7 months prior primarily originate from the middle and deep soil layers, whereas signals from 1 to 7 months prior are distributed throughout the entire soil column (Fig. 8c and g). When MLTSM is not more than 2 months, antecedent signals are mainly located in the shallow and middle soil layers in ERA5-Land and the entire soil column (MERRA-2) (Fig. 8d and h).

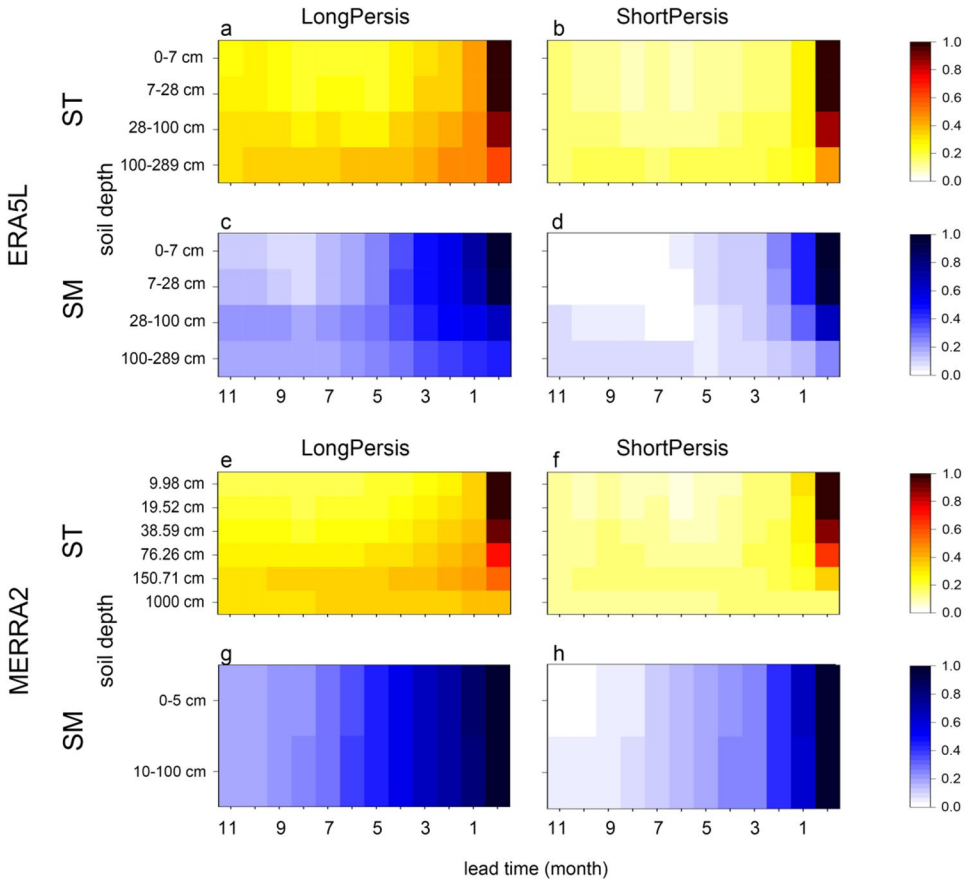

Fig. 8 The spatiotemporal mean of the correlation coefficients between antecedent SM/ST and current SM/SM, calculated across 12 months and all sites. **a**/**e** and **b**/**f** correspond to MLTST > 2 and MLTST ≤ 2, respectively. **c**/**g** and **d**/**h** correspond to MLTSM > 2 and MLTSM ≤ 2, respectively

On the whole, for MLTST and MLTSM shorter than 2 months, antecedent significant anomaly signals are distributed across the whole soil column, concentrated mainly in the shallow and middle soil layers. For MLTST greater than 2 months, the signals antecedent to more than 5 months are from deep soil and 2-to-5-month antecedent signals originate from middle and deep soil layers. For MLTSM greater than 2 months, the signals with a lead time of more than 7 months are mainly sourced from the middle and deep soil layers, and 2-to-7-month antecedent signals span the entire soil column, especially in the shallow and middle soil layers (Fig. 8). The antecedent signals that are significantly correlated with current ST or SM mainly originate from the middle and deep soil layers. This is because atmospheric forcing has a stronger influence on shallow soil than on deeper layers.

3.3 The spatial distribution and seasonal variation of ASTFlux and ASMFlux

Antecedent SM and ST can modulate current SM and ST of the first soil layer through the storage and propagation of anomaly signals in the soil, and then current SM and ST in the first soil layer can affect current surface fluxes, including SH, LH, emittedLW and etc. Using reanalysis data, the relationships between the SM/ST at the four soil layers and the concurrent SH, LH and emittedLW were analyzed using Pearson correlation coefficients (Fig. 3). As shown in Fig. 3, in both ERA5-Land and MERRA-2, the relationships of ST with subsequent surface fluxes exhibit similar patterns, as do those of SM. Moreover, due to the similar interannual variations of the ST/SM across soil layers, the linear correlations between the ST/SM in different soil layers and surface fluxes show similar monthly variations. And the ST/SM of the first soil layer exhibits the strongest correlations with surface fluxes (Fig. 3).

SH is primarily governed by the difference between SKT and T2m, while emittedLW depends primarily on SKT. SH is monotonically increasing with SKT, and emittedLW also increases monotonically with the difference between SKT and T2m. It should be noted that the method serves the purpose. The correlation coefficients used for spatial averaging reflect the consistency of the temporal variations between these variables, and a lower spatial average indicates poorer consistency in temporal variations between the reanalysis data and observational data in some regions. The values in Fig. 9 serve as an indicator of the relative performance of the two reanalysis datasets for the whole of China. The

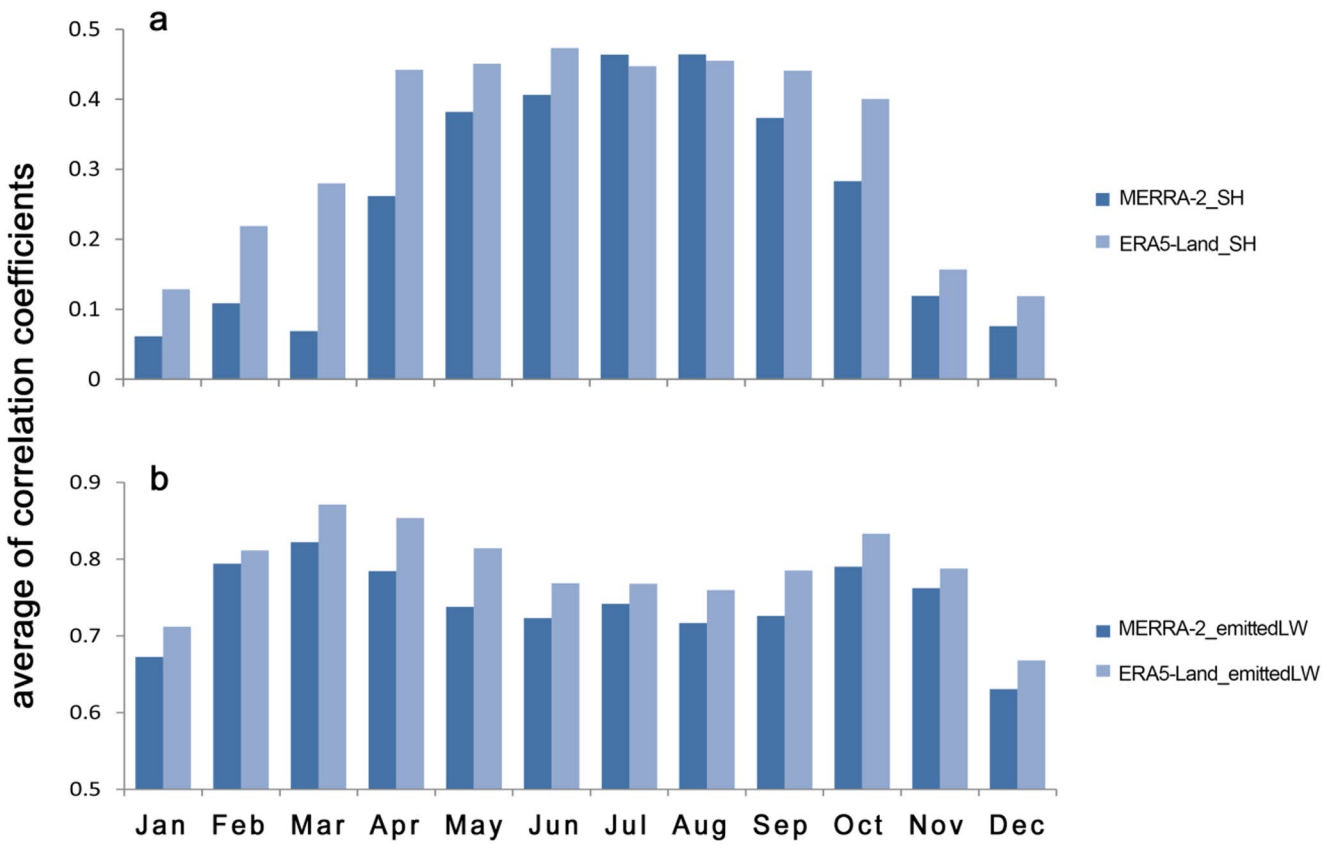

Fig. 9 The spatial average of the correlation coefficients between the reanalysis data and observed data. **a** Represents the correlations between the reanalysis SH and the observed SKT minus T2m. **b** Represents the correlations between the reanalysis emittedLW and the observed SKT

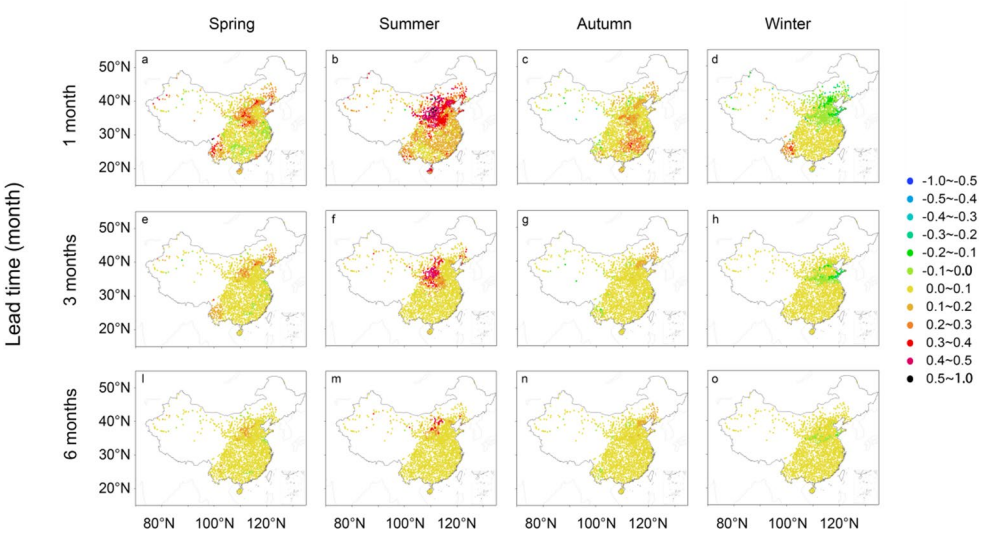

Fig. 10 Contributions of ST at different lead times to current SH anomalies in ERA5-Land. The first, second, third and fourth columns correspond to spring, summer, autumn and winter, respectively. The first, second and third rows correspond to lead times of 1 month, 3 months and 6 months, respectively

ERA5-Land and MERRA-2 SH data can capture the temporal variations in observed SKT minus T2m except November through March, and the spatial average of the correlation coefficients spans from 0.06 to 0.46 (Fig. 9a). The spatial average of correlation coefficients between reanalysis emittedLW and observed SKT ranges from 0.63 to 0.87 across 12 months (Fig. 9b). Additionally, the SH and emittedLW data from ERA5-Land exhibit better consistency with the temporal variation characteristics of observational data than those from MERRA-2 overall. Therefore, in the analysis of the relationships between land surface fluxes and antecedent ST/SM, emphasis is placed on using ERA5-Land data.

The impact of antecedent ST on SH differs across different regions and throughout different seasons (Fig. 10).

The impact decreases successively from summer to spring, from spring to autumn, from autumn to winter. The differences across four seasons manifest in Area1. In spring, 1-month antecedent ST anomalies contribute from 0 to 40% to SH anomalies in western Area1, from − 10 to 10% in the areas south of 30°N, from 10 to 50% in southwest China, and from 10 to 30% in the coastal areas of southeast China (Fig. 10a). 3-month antecedent ST anomalies have a relatively reduced impact on SH anomalies, and contribute more than 10% to SH anomalies in the northern and western parts of Area1, as well as in southwest China in spring (Fig. 10e). 6-month antecedent ST anomalies account for less than 10% of SH anomalies (Fig. 10l). In summer, 1-month antecedent ST anomalies contribute from 30 to 50% to SH anomalies in most of Area1. In the areas south of 30°N, the contribution ranges from 0 to 30%, with from 20 to 30% in most areas within this region (Fig. 10b). With the exception of the western area of Area1, where the contribution of 3-month antecedent ST anomalies to SH anomalies ranges from 20 to 50%, the contribution in the remaining areas is between 0 and 10% (Fig. 10f). The contribution of 6-month antecedent ST anomalies to SH anomalies are mainly less than 10%, with the contribution is concentrated within the 10–50% range in the western parts of Area1. In autumn, 1-month antecedent ST anomalies contribute from 0 to 30% to SH anomalies (Fig. 10c). The contributions of 3-month and 6-month antecedent ST anomalies mainly lie in the 0–10% range (Fig. 10g and n). In winter, the contributions of 1-month, 3-month and 6-month antecedent ST anomalies to SH anomalies are mainly between − 10 and 10%. In one word, antecedent positive ST anomalies can lead to positive SH anomalies, and the contribution of antecedent ST anomalies to SH anomalies is higher in summer and spring, especially in Area1. SH largely governs the coupling strength between ST and T2m. As shown in Fig. 10, the spatial pattern of the relationship between ST and SH is consistent with the pattern of ST–T2m coupling strength reported by Li et al (2022).The impact of antecedent SM on SH varies with regions and seasons (Fig. 11). The contribution of antecedent SM anomalies to SH anomalies is mainly between − 10 and 10% in Area2. Moreover, when the lead time is 1 month, the contribution ranges from − 10 to -50%. The contribution of antecedent SM anomalies to SH anomalies is higher in winter and spring. When the lead time is 3 and 6 months, the contribution of antecedent SM anomalies to SH anomalies is very small, with the exception of the four sites in the western part of Area2, consistent with the spatial characteristics of MLTSM (Fig. 7).

The impact of antecedent ST on LH differs across different regions and throughout different seasons (Fig. 12). In spring and summer, the LH anomalies caused by positive antecedent ST anomalies are negative and positive in Area1 and the remaining area, respectively. Moreover, the impact of antecedent ST on LH is greater in summer and spring than in autumn and winter. In spring, the contribution of 1-month antecedent ST anomalies to LH anomalies exhibits distinct regional variations: in Area1, the contribution is from 0 to − 30%; in the southwest part of China, it spans from − 10 to − 40%; and in the remaining area, it is from 0 to 30% (Fig. 12a). The contribution of 3-month antecedent ST anomalies predominantly ranges from − 10 to 10%, except for the southwest parts of China and some parts of Area1, where the contribution is about – 10–20% (Fig. 12e). The contribution of 6-month antecedent ST anomalies is predominantly within the interval of 0 to 10% (Fig. 12l). In summer, the contribution is mainly from − 10 to − 50% in Area1, and the contribution is mainly from 0 to 50% in the middle and upper reaches of the Yangtze River. In the areas south of 25°N, the contribution ranges from 0 to 40% (Fig. 12b). 3-month antecedent ST anomalies account for 10–50% of negative LH anomalies in western Area1. Between 105° E–110° E and 30° N–35° N, 3-month antecedent ST anomalies contribute 10–50% to LH anomalies; in the remaining area, the contribution remains within the 0–10% range (Fig. 12f). 6-month antecedent ST anomalies contribute − 10 to − 50% in the western parts of Area1, and predominantly contribute less than 10% in the remaining areas (Fig. 12m). In autumn, 1-month antecedent ST anomalies contribute 0 to − 20% to LH anomalies in the region of 115° E–120° E and 25° N–45° N, and contribute less than 10% to LH anomalies in the remaining areas (Fig. 12c). 3-month and 6-month antecedent ST anomalies contribute less than 10% to LH anomalies in the areas north of 35°N and east of 110°E, and contribute less than 10% in the remaining areas (Fig. 12g and m). In winter, the contribution of 1-month antecedent ST anomalies is from 0 to 30% in the parts of Area1, is from 0 to − 30% in the southwestern China, and is less than 10% in the remaining areas (Fig. 12d). 3-month antecedent ST anomalies contribute 10% to 30% to LH anomalies in the region of 115° E–120° E and 33° N–36° N, and contribute less than 10% in the remaining areas. 6-month antecedent ST anomalies contribute less than 10% to LH anomalies. In one word, antecedent positive ST anomalies can lead to negative LH anomalies in Area1, and the contributions of antecedent ST anomalies to LH anomalies decrease with lead time. Additionally, 1-month positive antecedent ST anomalies lead to positive LH anomalies in summer.

The impact of antecedent SM on LH is stronger in spring, autumn and winter than in summer, and positive SM anomalies can lead to positive LH anomalies in Area2 (Fig. 11). In spring, 1-month antecedent SM anomalies contribute 0% to 40% to LH anomalies. 3-month and 6-month antecedent SM anomalies contribute less than 10% to LH anomalies

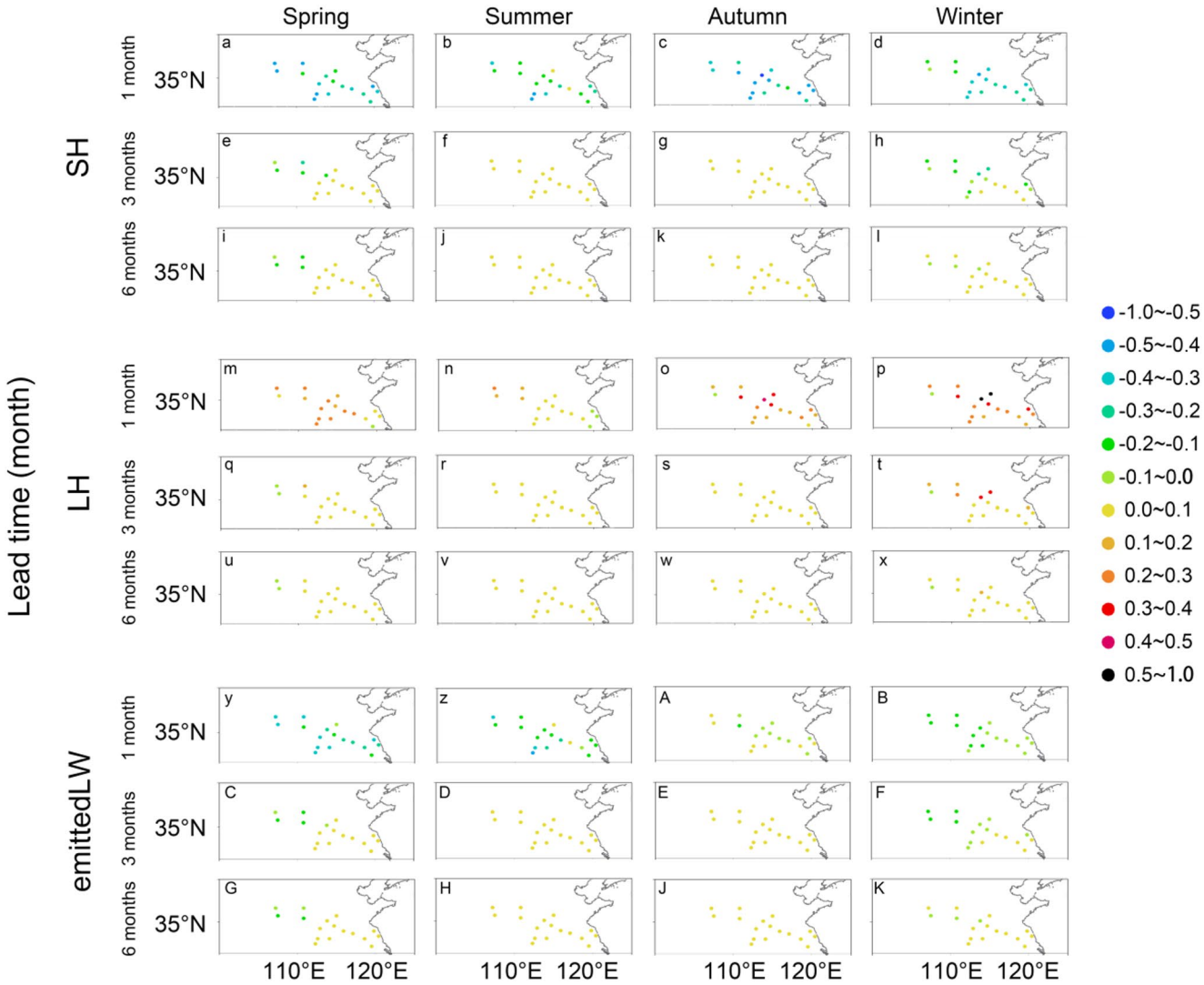

Fig. 11 Contributions of SM at different lead times to current SH/LH/emittedLW anomalies in ERA5-Land. The first, second, third and fourth columns correspond to spring, summer, autumn and winter, respectively. The first, second and third rows correspond to lead times of 1 month, 3 months and 6 months, respectively

(Fig. 11q and u). In summer, the contributions of 1-month, 3-month and 6-month antecedent SM anomalies to LH anomalies are primarily less than 10% (Fig. 11n, r and v). In autumn, 1-month antecedent SM anomalies contribute 10–50% to LH anomalies (Fig. 11o). 3-month and 6-month antecedent SM anomalies contribute less than 10% to LH anomalies (Fig. 11s and w). In winter, 1-month antecedent SM anomalies contribute 20% to over 50% to LH anomalies (Fig. 11p). 3-month antecedent SM anomalies contribute 0–40% to LH anomalies, while 6-month antecedent SM anomalies predominantly contribute less than 10% to LH anomalies (Fig. 11x).

The impact of antecedent ST on emittedLW show similar characteristics to the impact of antecedent ST on SH, and the impact is significantly stronger in summer and spring than in winter and autumn (Fig. 13). Positive antecedent ST anomalies facilitate the occurrence of positive emittedLW anomalies. In spring, the contribution of antecedent ST anomalies to emittedLW anomalies exhibit distinct regional variations: in Area1, the contribution is from 10% to over 50%; in the southwest part of China, it spans from 10 to 50%; in the eastern coastal areas, it ranges from 30 to 40%; and in the remaining area, it is mainly from 10 to 30% (Fig. 13a). The contribution of 3-month antecedent ST anomalies predominantly ranges from 10 to 50% in the western and northern parts of Area1. The contribution mainly varies from 0 to 10% in the remaining areas, except for the southwest and southeast part of China, where it is about 10% to 20% (Fig. 13e). The contribution of 6-month antecedent ST anomalies is from 0% to over of 50%, and it mainly ranges from 0 to 10% in the remaining areas (Fig. 12l). In summer, the contribution of 1-month antecedent ST anomalies

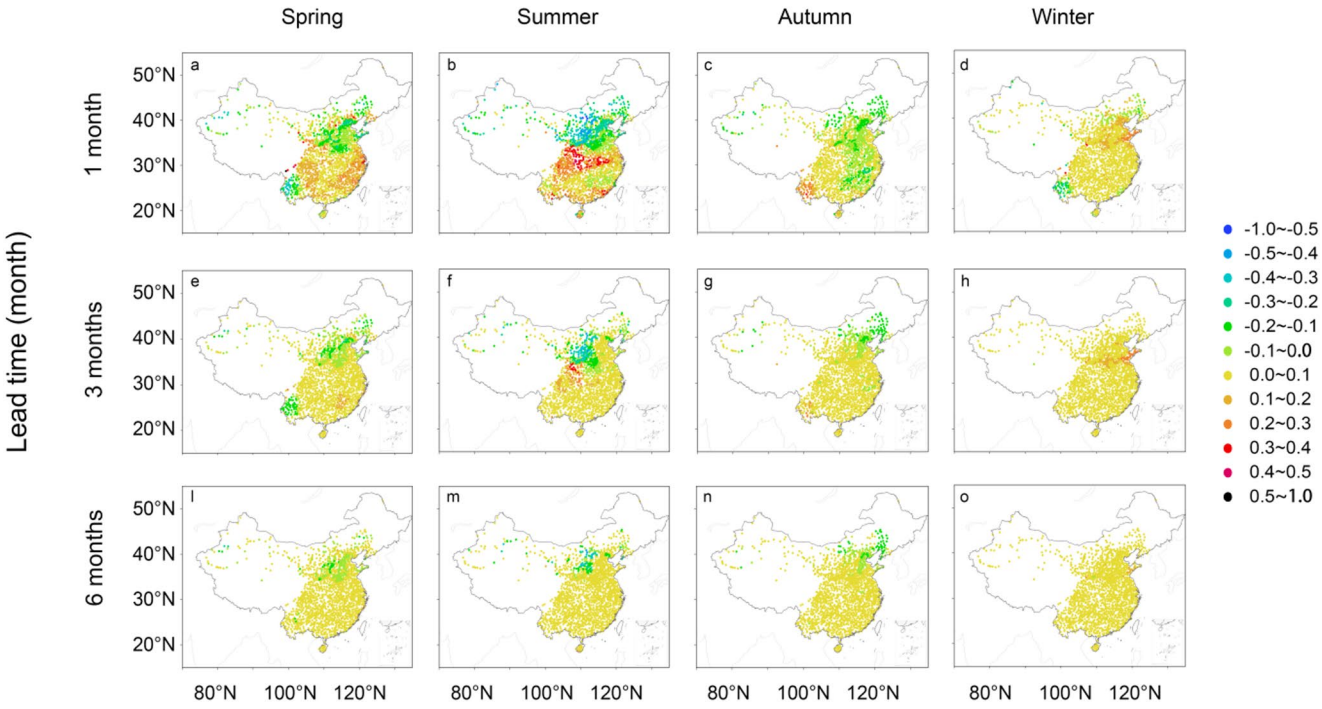

Fig. 12 Contributions of ST at different lead times to current LE anomalies in ERA5-Land. The first, second, third and fourth columns correspond to spring, summer, autumn and winter, respectively. The first, second and third rows correspond to lead times of 1 month, 3 months and 6 months, respectively

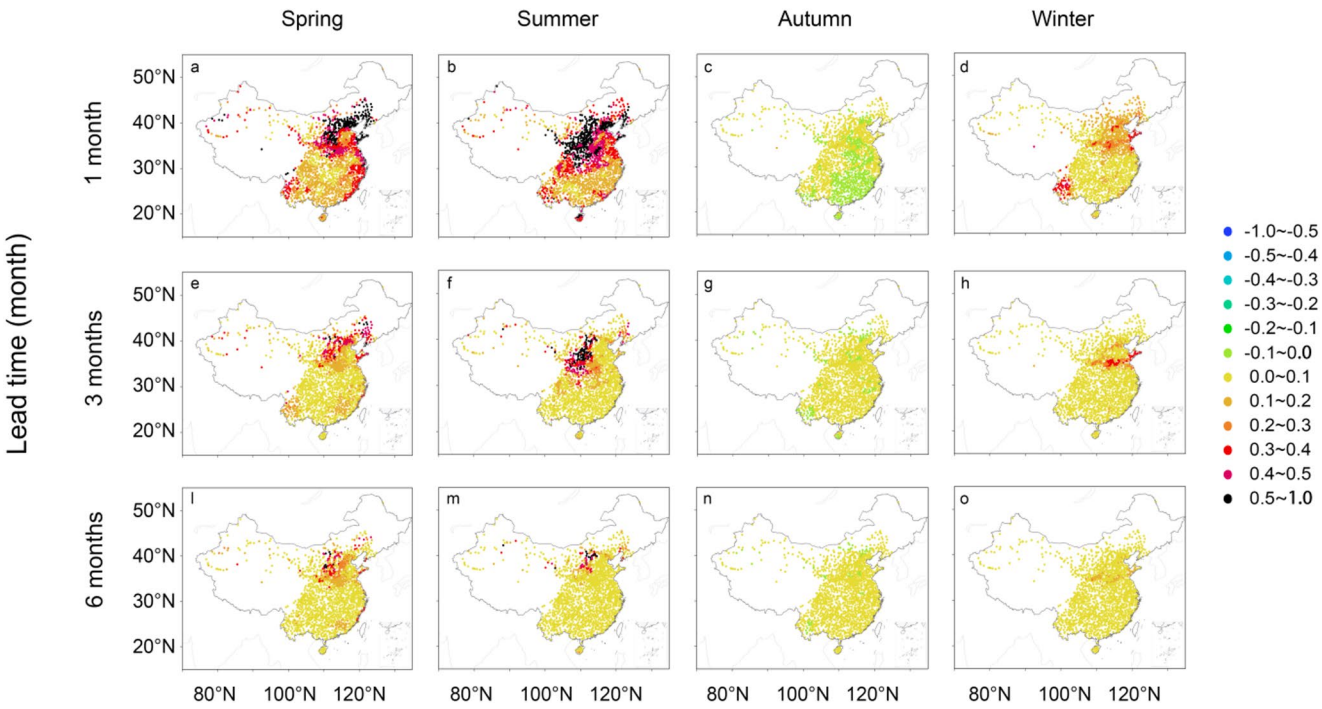

Fig. 13 Contributions of ST at different lead times to current emittedLW anomalies in ERA5-Land. The first, second, third and fourth columns correspond to spring, summer, autumn and winter, respectively. The first, second and third rows correspond to lead times of 1 month, 3 months and 6 months, respectively

is mostly higher than 20%, and it is from 30% to over of 50% in Area1, Hainan Island, the southwest part of China and the coastal areas of Guangdong province (Fig. 13b). 3-month antecedent ST anomalies contribute 20% to over 50% in the western part of Area1, and contribute mainly less than 10% in the remaining areas (Fig. 13f). The contribution of 6-month antecedent ST anomalies is merely less than 10%, with the exception of certain parts of Area1, where it ranges from 10% to over 50% (Fig. 13m). In autumn, 1-month, 3-month and 6-month antecedent ST anomalies contribute less than 10% to emittedLW anomalies (Fig. 13c, g and n). In winter, the contribution of 1-month antecedent ST anomalies ranges from 10 to 40% in Area1 and the southwest part of China (Fig. 13d), while it is less than 10% in the remaining areas. 3-month antecedent ST anomalies contribute 10–40% to emittedLW anomalies in the region of 115°E-120°E and 33° N–36° N, and contribute less than 10% in the remaining areas. 6-month antecedent ST anomalies contribute less than 10% to emittedLW anomalies. In one word, antecedent positive ST anomalies can lead to positive emittedLW anomalies in Area1, and the contributions of antecedent ST anomalies to emittedLW anomalies decrease with lead time. Moreover, the contribution of antecedent ST anomalies to emittedLW anomalies is greater in spring and summer than in winter and autumn.

The impact of antecedent SM on emittedLW varies with regions and seasons (Fig. 11). When the lead time is 1 month, the contribution ranges from − 10 to − 40% in spring, from − 10 to − 50% in summer, from 10 to − 10% in autumn, and from 0 to − 10% in winter. The contribution of antecedent SM anomalies to emittedLW anomalies is higher in summer and spring. When the lead time is 3 and 6 months, the contribution of antecedent SM anomalies to emittedLW anomalies is very small, with the exception of the four sites in the western part of Area2, consistent with the spatial characteristics of MLTSM (Fig. 11).

Given the close couplings between ST/SM and SH/LH/emittedLW, the impact of antecedent ST/SM on these fluxes is largely governed by the memory of ST and SM anomalies. Consequently, the spatial patterns of the flux anomalies associated with ST/SM are highly consistent with those of MLTST and MLTSM.

3.4 The simulated influence of ST and SM on subsequent land surface fluxes

Based on the simulations conducted with the WRF4.3 model, the influence of ST and SM on subsequent surface fluxes was analyzed. To better evaluate model performance, the year 2023 was selected as a case study. As shown in Figure S2, the WRF-simulated T2m and Rainfall generally capture the spatial patterns and magnitude of the observed values, with T2m showing particularly good agreement. However, the simulated T2m in January is significantly lower than observed, particularly in the dry–wet transition zones, with differences reaching up to 8 °C. The simulated July T2m is underestimated in southern regions but overestimated in northern regions, with cold biases reaching 8 °C and warm biases up to 6 °C. Simulated precipitation in both January and July is notably underestimated, especially in the Yangtze-Huai and southeastern regions, with deficits reaching 20 mm and 200 mm in January and July, respectively. The simulation biases may lead to inaccuracies in the calculation of the memory of ST/SM anomalies and the influence of ST/SM on subsequent surface fluxes derived from the model results. Although the model captures the spatial patterns of temperature and precipitation reasonably well, its simulation of their magnitudes is less accurate, which is consistent with previous studies (Kong et al. 2019, 2020; Gao 2020).

The MLTST and MLTSM depend on the persistence time of ST and SM anomalies, respectively. As shown in Fig. 14, the simulated persistence of SM anomalies exceeds 9 months in most areas. Compared to the simulated persistence of SM anomalies, the MLTSM derived from reanalysis data is significantly shorter, particularly in ERA5-Land. The simulated persistence of ST anomalies exceeds 6 months in the regions of (20° N–27° N, 107° N–115° N), (32° N–38° N, 105° N–115° N) and parts of Northeast China. However, the MLTST derived from both MERRA-2 and ERA5-Land in the region (20° N–27° N, 107° N–115° N) is noticeably shorter. The long MLTST derived from MERRA-2 in the region (27° N–35° N, 103° N–120° N) is not reflected in the simulated persistence time of ST anomalies. Moreover, the long MLTST both in MERRA-2 and ERA5-Land is also not reflected in the simulated persistence time of ST anomalies in Yunnan province. Additionally, both the simulated persistence time of ST anomalies and the MLTST derived from ERA5-Land exhibit high values in the region (32° N–38° N, 105° N–115° N). In short, the regions exhibiting high values in the simulated ST persistence and the MLTST are not fully consistent. The MLTST from ERA5-Land shows better agreement with the simulated ST persistence in northern areas than that from MERRA-2.

Based on the simulations, the maximum lag time at which ST and SM anomalies can still affect SH, LH and emittedLW (MLTST-SH/MLTST-LH/MLTST-emittedLW/MLTSM-SH/MLTSM-LH/MLTSM-emittedLW) were analyzed. The spatial patterns of the influence of ST on subsequent surface fluxes (ASTFlux) are approximately consistent with those of the persistence time of ST anomalies (Fig. 15). Positive ST anomalies contribute to increased SH, and the influence of ST on subsequent SH decrease rapidly over time, and the strength of the influence in both ERA5-Land and

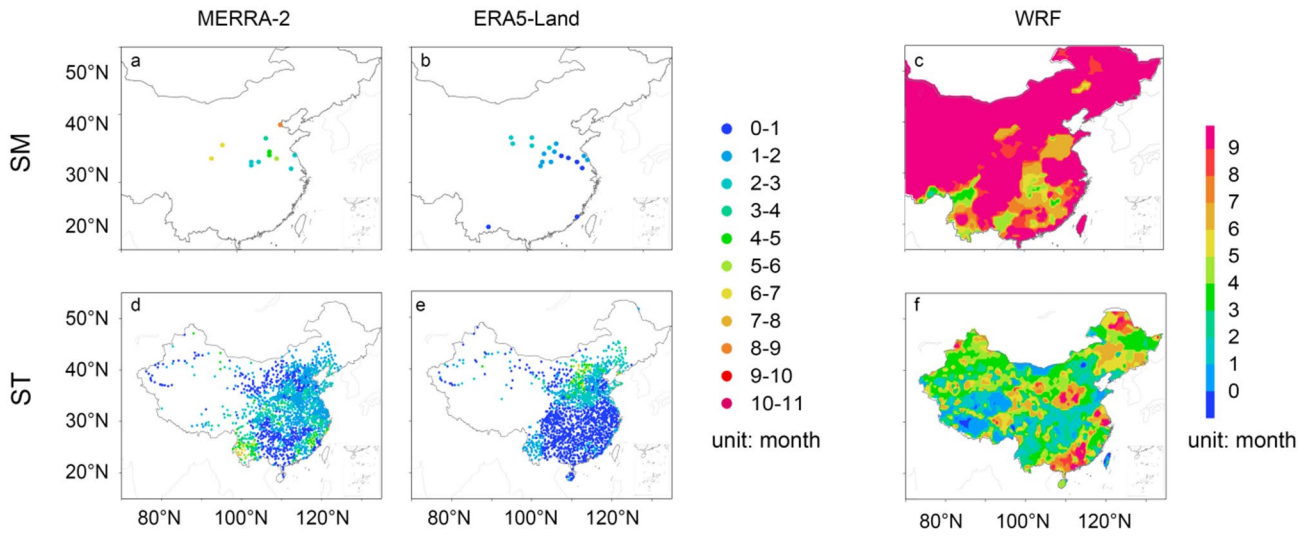

Fig. 14 The spatial distributions of the MLTSM (**a**, **b**) and MLTST (**d**–**e**). **c** and **f** are the memory time of SM and ST anomalies obtained from the simulations. **a** and **d** are obtained from the MERRA-2 data, while **b** and **e** are obtained from the ERA5-Land data

MERRA-2 exhibits a "high-low–high" spatial pattern from north to south within the region (20° N–40° N, 105° N–120° N), which is consistent with the MLTST-SH derived from simulations (Fig. 15a–g).

Positive ST anomalies contribute to decreased LH, and the influence of ST on subsequent LH decrease rapidly over time, and the strength of the influence in MERRA-2 exhibits a "high-low–high" spatial pattern from north to south within the region (20° N–40° N, 105° N–120° N), which is consistent with the MLTST-LH derived from simulations. Moreover, the influence in ERA5-Land is stronger north of 35°N, and the regions with high MLTST-LH can't be found in those in ERA5-Land. Additionally, the regions where the influence value ranges from 10 to 20% are largely consistent with those where MLTST-LH exceeds 6 months within the region (32° N–38° N, 105° N–115° N) (Fig. 15h–n).

The spatial patterns of ASTFlux-emittedLW in MERRA-2 and ERA5-Land exhibit similar features, and the values in ERA5-Land are higher than those in MERRA-2 for regions north of 35°N and lower for regions to south. The influence of ST on emittedLW at a one-month lag in ERA5-Land shows spatial similarity to MLTST-emittedLW in the simulations, except in Yunnan province, and the areas with high values in ERA5-Land are more extensive than those with high values of MLTST-emittedLW in the simulations. Moreover, the areas with high values of MLTST-emittedLW in the region (32° N–38° N, 105° N–115° N) are broadly consistent with those with high values in ERA5-Land, and the high-value areas of MLTST-emittedLW in southeastern China are not found in both ERA5-Land and MERRA-2.

In summary, the areas exhibiting a strong influence of ST on subsequent surface fluxes in ERA5-Land are broadly consistent with the regions characterized by high MLTST values between 35°N and 40°N in the simulations. The area characterized by high MLTST values in southeastern China is not reflected in the spatial patterns of ST influence on subsequent surface fluxes in ERA5-Land and MERRA-2.

The influence of SM on subsequent surface fluxes (ASMFlux) exhibits similar spatial patterns and temporal variations between ERA5-Land and MERRA-2. The spatial patterns of the influence of SM on subsequent surface fluxes in the simulations are broadly consistent with those of the ASMFlux in ERA5-Land and MERRA-2 (Fig. 16). In most parts of the region (20°N-40°N, 100°N-120°N), the maximum lag time at which SM can influence surface fluxes exceeds 6 months, particularly for SH and LH. Moreover, the west-strong-east-weak spatial pattern of the influence of SM on subsequent surface fluxes in the simulations is broadly consistent with that of ASMFlux in ERA5-Land and MERRA-2.

4 Conclusion and discussion

This study focuses on the impact of antecedent SM and ST on current land surface fluxes through modifying current SM and ST in China. Given the scarcity of ST and SM observation data, reanalysis data is evaluated and utilized. The reanalysis data include ERA5-Land, MERRA-2, NCEP and GLDAS. The four reanalysis ST and SM data was evaluated from the perspective of interannual variations. Compared to the other datasets, the interannual variations of ERA5-Land exhibit a greater similarity to observational data, regardless of whether the variable is ST or SM, followed by

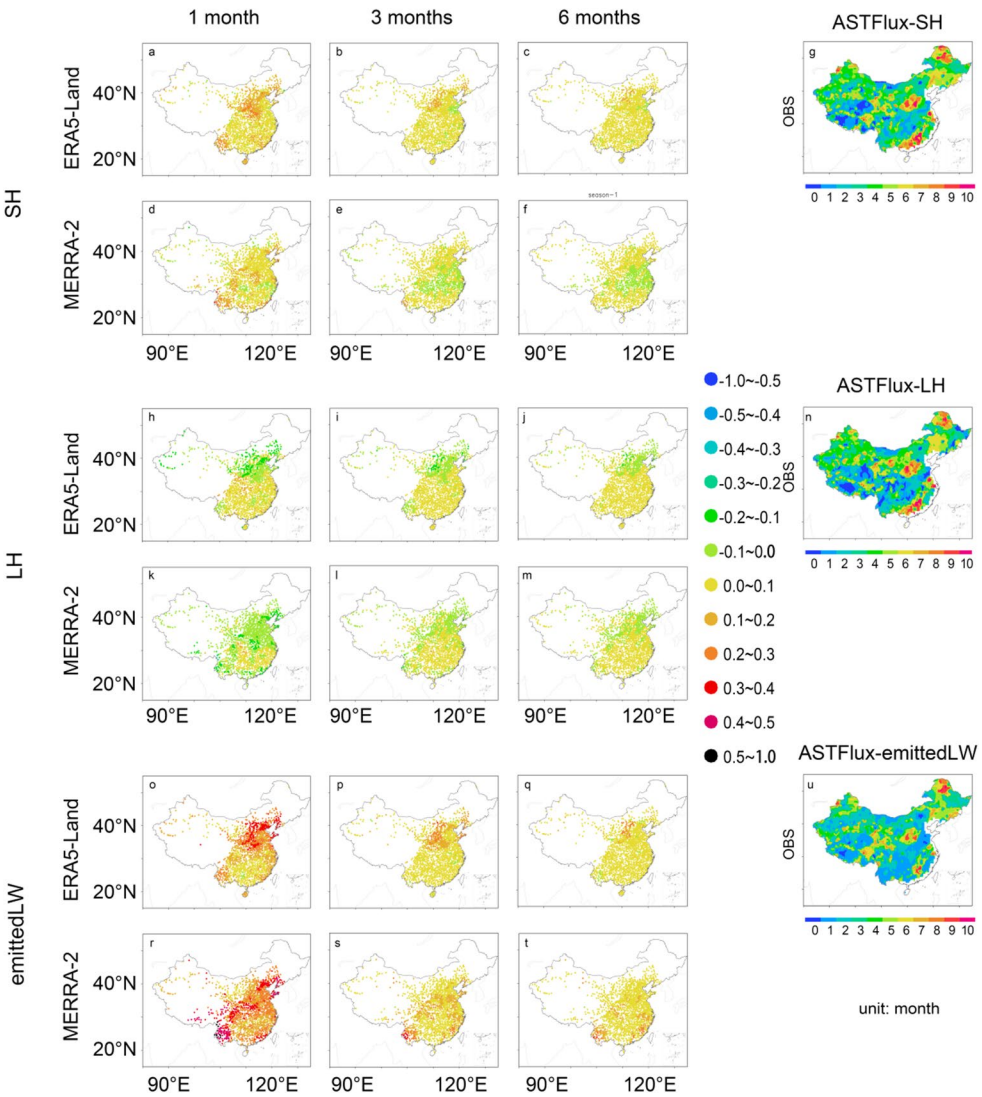

Fig. 15 The influences of antecedent ST on SH, LH and emittedLW. The left panels correspond to the contributions of ST at different lead times to current land surface flux anomalies (ASTFlux-SH/ASTFlux-LH/ASTFlux-emittedLW), all of which are derived from the reanalysis data. The right three panels show the maximum lag time at which ST can influence surface flux anomalies (MLTST), all derived from observational data

MERRA-2. Moreover, the monthly variations of the correlation between ST in different soil layers and surface fluxes exhibit consistent patterns, and the same holds true for SM. Additionally, the correlation characteristics between ST/SM and surface fluxes are largely consistent between ERA5-Land and MERRA-2. And among all soil layers, both the ST and SM in the first soil layer show the strongest correlation with surface fluxes. Therefore, particular emphasis was placed on the concurrent ST and SM in the first soil layer in relation to surface fluxes in the analysis. Based on the similarity in interannual variability with observational data, a subset of the ST and SM data from ERA5-Land and MERRA-2 was selected for further analysis.. ERA5-Land captures the spatial distribution and seasonal variability of the observation-based MLTST more accurately than MERRA-2. In ERA5-Land, MLTST exhibits greater values in summer and spring than in autumn and winter. Compared with other areas, MLTST is significantly greater in Area1 (33°N-42°N, 105°E-120°E), where it can reach up to 11 months. In winter, spring, summer and autumn, MLTSM ranges from 1 to 5 months, from 0 to 5 months, from 0 to 2 months, and from 0 to 2 months, respectively. The signals with a relatively long lead time that are closely related to the ST and SM of the first layer mainly come from deep soil layer. Both MERRA-2 and ERA5-Land indicate that the MLTSM decrease successively from winter to spring, spring to autumn, autumn to summer. Furthermore, the MLTSM is higher in the western part than in the eastern part of the Area2. However, notable differences exist between the MLTSM values derived from MERRA-2 and those from ERA5-Land.

Moreover, in terms of temporal variability, SH and emittedLW data from ERA5-Land demonstrate stronger agreement with observations than those derived from MERRA-2. Using ERA5-Land data, positive antecedent ST anomalies mainly lead to positive SH anomalies, negative LH

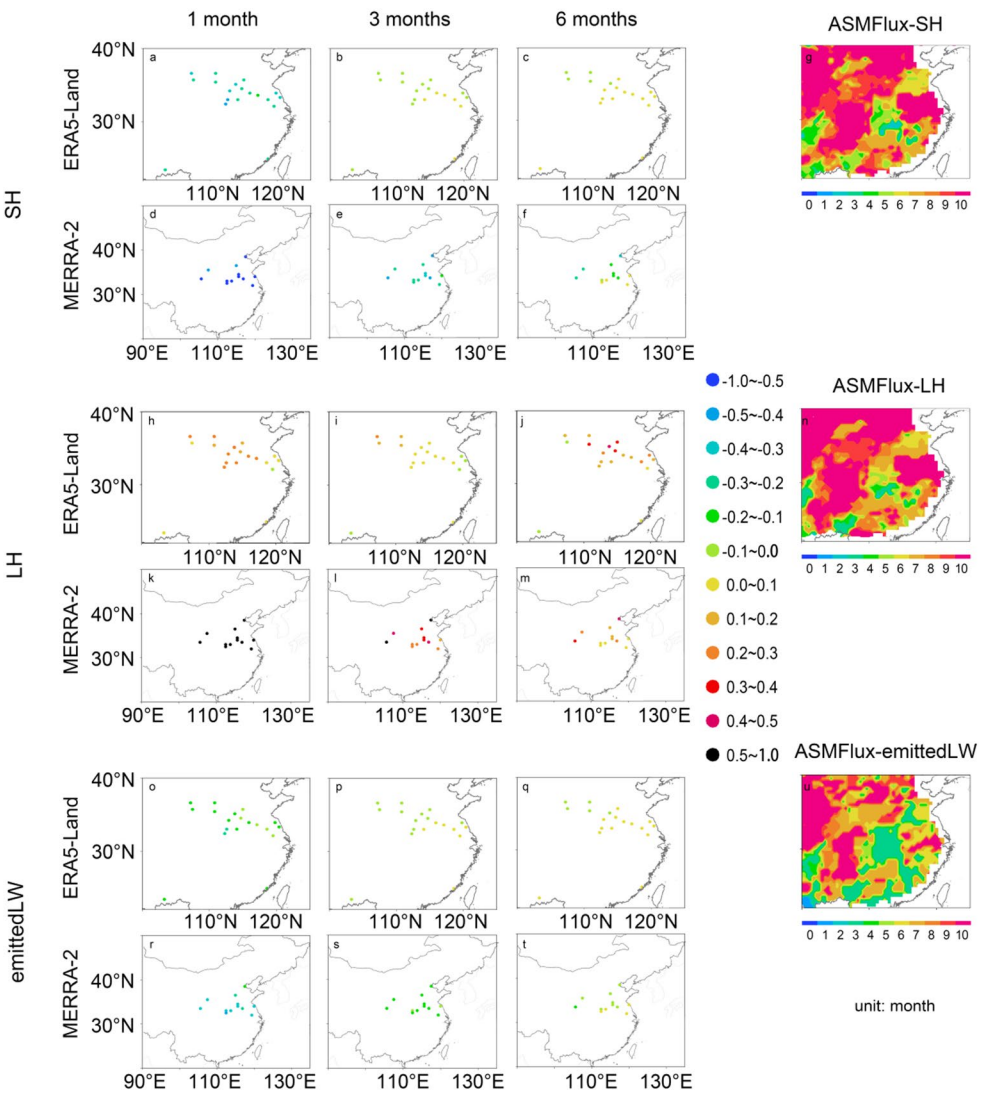

Fig. 16 The influences of antecedent SM on SH, LH and emittedLW. The left panels correspond to the contributions of SM at different lead times to current land surface flux anomalies (ASMFlux-SH/ASMFlux-LH/ASMFlux-emittedLW), all of which are derived from the reanalysis data. The right three panels show the maximum lag time at which SM can influence surface flux anomalies (MLTSM), all derived from observational data

anomalies and positive emittedLW anomalies. In contrast, positive antecedent SM anomalies mainly result in negative SH anomalies, positive LH anomalies and negative emittedLW anomalies. Using ERA5-Land data, the areas with high ASTFlux values are broadly consistent with regions characterized by high MLTST, and the impact of antecedent ST on surface fluxes is significantly more intense in Area1 than in the remaining areas, and the impact of antecedent ST on surface fluxes decreases from summer and spring to autumn and winter. The contribution of antecedent SM anomalies to SH and LH anomalies is higher in winter, autumn and spring than in summer, and the impact of antecedent SM on surface fluxes is stronger in the western part of Area2 than in the other regions. The contribution of antecedent SM anomalies to emittedLW anomalies is higher in summer and spring than in autumn and winter.

The WRF-simulated T2m and rainfall generally capture the spatial patterns and magnitude of the observed values; however, substantial discrepancies exist in certain regions. The biases of the simulations could affect the accuracy of the MLTST/MLTSM and the influence of ST/SM on subsequent surface fluxes derived from the simulations. The regions exhibiting high values in the simulated ST persistence and the MLTST from ERA5-Land and MERRA-2 are not entirely spatially consistent. The MLTST from ERA5-Land shows better agreement with the simulated ST persistence in Area1 than that from MERRA-2. Moreover, with the exception of southeastern China, the areas exhibiting high MLTST values in the simulations are broadly consistent with Area 1, where is characterized by high ASTFlux values in ERA5-Land. However, the region of high MLTST values in southeastern China in the simulations is not reflected in the spatial distribution of high ASTFlux in either ERA5-Land or MERRA-2, and this region is not reflected in the MLTST derived from the observations. The west-strong-east-weak spatial pattern of the influence of SM

on subsequent surface fluxes in the simulations is broadly consistent with that of ASMFlux in ERA5-Land and MERRA-2. In short, the MLTST and ASTFlux in ERA5-Landshow closer spatial agreement with the simulations, and the east-low–west-high pattern of MLTSM and AST-Flux is also partly reflected in the simulations. Due to the scarcity of observational data and the differences between the reanalysis data and the observational data, MLTST and ASTFlux were not analyzed in the western part of China, northeast China, and the analysis of MLTSM and ASMFlux were only carried out in Area2 (32°N-37°N, 105°E-122°E). Moreover, the biases of the simulation using WRF4.3 could affect the accuracy of the calculation of the persistence of ST/SM anomalies, as well as the influence of ST/SM on subsequent surface fluxes derived from the simulations. Cross-validation results reveal that Area1 is characterized by high MLTST and strong ASTFlux. Due to the scarcity of the SM observation data, the persistence of SM anomalies and their influence on subsequent surface fluxes derived from reanalysis data have not been sufficiently validated. However, the MLTSM and ASMFlux from ERA5-Land are spatially similar to those from MERRA-2. In this study, the important effect of ST/SM anomalies on emittedLW/LH/SH several months later are confirmed, and the purpose of this study is to understand clearly the potential of ST/SM to affect subsequent atmosphere through the impact of ST/SM anomaly persistence on subsequent surface fluxes. As one of the crucial processes, the influence of land surface fluxes on the local and remote atmosphere is highly complex, exhibiting significant temporal and spatial heterogeneity, and calls for in-depth research.

Supplementary Information The online version contains supplementary material available at https://doi.org/10.1007/s00382-026-08098-z.

Acknowledgements This work was supported by the National Natural Science Foundation of China (Grant 42130609, 41975081 and 41005047).

Availability of data and materials The site data of soil temperature, precipitation and air temperature is from the China National Stations' Fundamental Elements Data sets V3.0 (National Meteorological Information, 2019), which can be obtained from: http://data.tpdc.ac.cn/en/data/52c77e9c-df4a-4e27-8e97-d363fdfce10a/, and is also available at http://101.200.76.197/en/?r=data/detail%26dataCode=SURF_CLI_CHN_MUL_DAY_CES_V3.0. Soil moisture data is from the China Meteorological Data Service Centre, which can be obtained from: http://www.nmic.cn/data/cdcdetail/dataCode/SK.1471.001.html, http://www.nmic.cn/data/cdcdetail/dataCode/SK.1472.001.html. ERA5 reanalysis data is from https://cds.climate.copernicus.eu/cdsapp#!/search?type=dataset%26text=ERA5.GLDAS reanalysis data is from https://ldas.gsfc.nasa.gov/gldas. NCEP-DOE Reanalysis II data is from https://psl.noaa.gov/data/gridded/data.ncep.reanalysis2.html. MERRA-2 data is from https://disc.gsfc.nasa.gov/datasets/M2T1NXLND_5.12.4/summary?keywords=MERRA-2. The meteorological dataset was sourced from the China Meteorological Data Service Centre through its product tailoring services. The full product details are accessible through the following link: http://data.cma.cn/en/?r=article/getLeft/id/343/keyIndex/30.

Declarations

Conflict of interest The authors have no relevant financial or non-financial interests to disclose.

References

Alfaro E, Gershunov A, Cayan D (2006) Prediction of summer maximum and minimum temperature over the Central and Western United States: the role of soil moisture and sea surface temperature. J Clim 19(8):1407–1421. https://doi.org/10.1175/JCLI3665.1

Beljaars A, Viterbo P, Miller M, Betts A (1996) The anomalous rainfall over the United States during July 1993: sensitivity to land surface parameterization and soil moisture anomalies. Mon Weather Rev 124(3):362–383. https://doi.org/10.1175/1520-0493%281996%29124%3C0362:TAROTU%3E2.0.CO;2

Dirmeyer PA (2011) The terrestrial segment of soil moisture–climate coupling. Geophys Res Lett 38:L16702. https://doi.org/10.1029/2011GL048268

Dirmeyer PA, Schlosser CA, Brubaker KL (2009) Precipitation, recycling, and land memory: an integrated analysis. J Hydrometeorol 10(1):278–288. https://doi.org/10.1175/2008JHM1016.1

Dirmeyer PA, Wang Z, Mbuh MJ, Norton HE (2014) Intensified land surface control on boundary layer growth in a changing climate. Geophys Res Lett 41:1290–1294. https://doi.org/10.1002/2013GL058826

Dong YS, Chen HS, Dong X (2023) Impact of antecedent soil moisture anomalies over the Indo-China Peninsula on the super Meiyu event in 2020. J Meteorol Res 37(2):234–247. https://doi.org/10.1007/s13351-023-2144-4

Dorigo W, Wagner W, Albergel C, Albrecht F, Balsamo G, Brocca L et al (2017) ESA CCI soil moisture for improved Earth system understanding: state-of-the art and future directions. Remote Sens Environ 203(1):185–215. https://doi.org/10.1016/j.rse.2017.07.001

Fischer EM, Seneviratne SI, Vidale PL, Lüthi D, Schär C (2007) Soil moisture–atmosphere interactions during the 2003 European summer heat wave. J Clim 20(20):5081–5099. https://doi.org/10.1175/JCLI4288.1

Gao SB (2020) Dynamical downscaling of surface air temperature and precipitation using RegCM4 and WRF over China. Clim Dyn 55:1283–1302. https://doi.org/10.1007/s00382-020-05326-y

Gao CJ, Chen HS, Xu B (2014) Possible relationships among South China Sea SSTA, soil moisture anomalies in Southwest China and summer precipitation in Eastern China (in Chinese). J Trop Meteorol 29(1):228–235. https://doi.org/10.16555/j.1006-8775.2014.03.005

Gelaro R, McCarty W, Suarez MJ, Todling R, Molod A, Takacs L, Randles CA et al (2017) The modern-era retrospective analysis for research and applications, version 2 (MERRA-2). J Climate 30(14):5419–5454. https://doi.org/10.1175/JCLI-D-16-0758.1

Gómez I, Caselles V, Estrela MJ, Niclòs R (2016) Impact of initial soil temperature derived from remote sensing and NSFC 2024 numerical weather prediction datasets on the simulation of extreme heat events. Remote Sens Environ 8(7):589. https://doi.org/10.3390/rs8070589

Hersbach H, de Rosnay P, Bell B, Schepers D, Simmons A, Soci C et al (2018) Operational global reanalysis: progress, future directions

and synergies with NWP. ERA Rep Ser 27:65. https://doi.org/10.21957/tkic6g3wm
Hersbach H, Bell B, Berrisford P, Hirahara S, Horanyi A, Muñoz-Sabate J et al (2020) The ERA5 global reanalysis. Q J R Meteorol Soc 146(730):1999–2049. https://doi.org/10.1002/qj.3803
Kim H, Choi M (2015) Impact of soil moisture on dust outbreaks in East Asia: using satellite and assimilation data. Geophys Res Lett 42(8):2789–2796. https://doi.org/10.1002/2015GL063325
Kong X, Wang A, Bi X, Wei J (2020) Daily precipitation characteristics of RegCM4 and WRF in china and their interannual variations. Clim Res 82:97–115. https://doi.org/10.3354/cr01621
Kong X, Wang A, Bi X, Dong W (2019) Assessment of temperature extremes in China using RegCM4 and WRF. Adv Atmos Sci 36:363–377. https://doi.org/10.1007/s00376-018-8144-0
Krishnamurthy V (2019) Predictability of weather and climate. Earth Space Sci 6(7):1043–1056. https://doi.org/10.1029/2019EA000586
Krueger ES, Ochsner TE, Carlson JD, Engle DM, Twidwell D, Fuhlendorf SD (2016) Concurrent and antecedent soil moisture relate positively or negatively to probability of large wildfires depending on season. Int J Wildland Fire 25(6):657–668. https://doi.org/10.1071/WF15104
Koster R, Suarez M (2001) Soil moisture memory in climate models. J Hydrometeorol 2(6):558–570. https://doi.org/10.1175/1525-7541%282001%29002%3C0558:SMMICM%3E2.0.CO;2
Kumar S, Newman M, Wang Y, Livneh B (2019) Potential reemergence of seasonal soil moisture anomalies in North America. J Climate 32(10):2707–2734. https://doi.org/10.1175/JCLI-D-18-0540.1
Li K, Zhang J, Wu L, Yang K, Li S (2022) The role of soil temperature feedbacks for summer air temperature variability under climate change over East Asia. Earths Future 10(4):e2021EF002377. https://doi.org/10.1029/2021EF002377
Li MX, Wu PL, Ma ZG et al (2020) Changes in soil moisture persistence in China over the past 40 years under a warming climate. J Clim 33:9531–9550. https://doi.org/10.1175/JCLI-D-19-0900.s1
Lin Z, Zuo Z, Zhang R, Xiao D, You Q, Qiao L (2022) Persistence of soil enthalpy drives the winter and summer climate connection in the Tibetan Plateau. Geophys Res Lett 49(12):e2022GL098503. https://doi.org/10.1029/2022GL098503
Liu D, Yu Z, Zhang J (2015) Diagnosing the strength of soil temperature in the land atmosphere interactions over Asia based on RegCM4 model. Glob Planet Change 130:7–21. https://doi.org/10.1016/j.gloplacha.2015.03.007
Liu L, Zhang R, Zuo Z (2017) Effect of spring precipitation on summer precipitation in Eastern China: role of soil moisture. J Climate 30(22):9183–9194. https://doi.org/10.1175/JCLI-D-17-0028.1
Liu Y, Xue Y, Li Q, Lettenmaier D, Zhao P (2020) Investigation of the variability of near-surface temperature anomaly and its causes over the Tibetan Plateau. J Geophys Res Atmos 125(19):e2020JD032800. https://doi.org/10.1029/2020JD032800
Lorenz EN (1969) Three approaches to atmospheric predictability. Bull Am Meteorol Soc 50(5):345–349. https://doi.org/10.1175/1520-0477-50.5.345
Ma Z (1995) A preliminary analysis for the relationship between the anomalies of soil temperature and either of floods in the Yangtse-Huai river reaches and strong drought in south of Yangtse River in summer of 1991 (in Chinese). Plateau Meteorol 14:185–190
Mahanama SPP, Koster RD, Reichle RH, Suarez MJ (2008) Impact of subsurface temperature variability on surface air temperature variability: an AGCM study. J Hydrometeorol 9(4):804–815. https://doi.org/10.1175/2008JHM949.1
Mariotti A, Ruti PM, Rixen M (2018) Progress in subseasonal to seasonal prediction through a joint weather and climate community effort. NPJ Clim Atmos Sci 1(1):4. https://doi.org/10.1038/s41612-018-0014-z
Meng L, Long D, Quiring SM, Shen Y (2014) Statistical analysis of the relationship between spring soil moisture and summer precipitation in East China. Int J Climatol 34(5):1511–1523. https://doi.org/10.1002/joc.3780
Miralles D, Teuling A, Van Heerwaarden C, de Arellano JVG (2014) Mega-heat wave temperatures due to combined soil desiccation and atmospheric heat accumulation. Nat Geosci 7(5):345–349. https://doi.org/10.1038/ngeo2141
Orth R, Seneviratne SI (2017) Variability of soil moisture and sea surface temperatures similarly important for warm-season land climate in the Community Earth System Model. J Climate 30(6):2141–2162. https://doi.org/10.1175/JCLI-D-15-0567.s1
Prodhomme C, Doblas-Reyes F, Bellprat Q, Dutra E (2016) Impact of land-surface initialization on sub-seasonal to seasonal forecasts over Europe. Clim Dyn 47:919–935. https://doi.org/10.1007/s00382-015-2879-4
Quesada B, Vautard R, Yiou P, Hirschi M, Seneviratne SI (2012) Asymmetric European summer heat predictability from wet and dry southern winters and springs. Nat Clim Chang 2(10):736–741. https://doi.org/10.1038/nclimate1536
Santanello JA Jr, Dirmeyer PA, Ferguson CR, Findell KL, Tawfik AB, Berg A et al (2018) Land–atmosphere interactions: the LoCo perspective. Bull Am Meteorol Soc 99(6):1253–1272. https://doi.org/10.1175/BAMS-D-17-0001.1
Seneviratne SI, Corti T, Davin EL, Hirschi M, Jaeger EB, Lehner I et al (2010) Investigating soil moisture–climate interactions in a changing climate: a review. Earth Sci Rev 99:125–161. https://doi.org/10.1016/j.earscirev.2010.02.004
Skamarock W C, Klemp J B, Dudhia J, Gill D O, Barker D M, Duda M G, et al (2008) A description of the Advanced Research WRF version 3. NCAR Tech. Note NCAR/TN-4751STR, 113 pp. https://doi.org/10.5065/D68S4MVH
Song Y, Chen H, Wang L, Huang A, Gu W, Ma Y (2023) Soil temperature controls the month-to-month lead-lag correlations of near-surface air temperatures in the middle and lower reaches of the Yangtze River basin. J Geophys Res Atmos 128:e2023JD039036. https://doi.org/10.1029/2023JD039036
Song YM, Huang AN, Chen HS (2022a) The persistence and reemergence of atmospheric anomaly signals in soil temperature. J Geophys Res Atmos 127:e2022JD037218. https://doi.org/10.1029/2022JD037218
Song YM, Huang AN, Chen HS (2022b) The storage of antecedent precipitation and air temperature signals in soil temperature over China. J Hydrometeorol 23(3):377–388. https://doi.org/10.1175/JHM-D-21.0126.1
Tang M, Wang J, Zhang J (1987) A primary method for predicting the spring rainfall by the winter soil temperature depth 80 cm (in Chinese). Plateau Meteorol 6:244–255
Wang YH, Chen W, Zhang JY, Nath D (2013) Relationship between soil temperature in May over Northwest China and the East Asian summer monsoon precipitation. Acta Meteorol Sin 27(5):716–724. https://doi.org/10.1007/s13351-013-0505-0
Weisheimer A, Doblas-Reyes FJ, Jung T, Palmer T (2011) On the predictability of the extreme summer 2003 over Europe. Geophys Res Lett 38(5):L05704. https://doi.org/10.1029/2010GL046455
Xue Y, Diallo I, Li W, Neelin JD, Chu PC, Vasic R et al (2018) Spring land surface and subsurface temperature anomalies and subsequent downstream late spring-summer drought/floods in North America and East Asia. J Geophys Res Atmos 123(10):5001–5019. https://doi.org/10.1029/2017jd028246
Xue Y, Vasic R, Janjic Z, Liu YM, Chu PC (2012) The impact of spring subsurface soil temperature anomaly in the western U.S. on North American summer precipitation: a case study using regional climate model downscaling. J Geophys Res Atmos 117:D11103. https://doi.org/10.1029/2012JD017692

Yang J, Chen H, Song HY et al (2021) Atmospheric circumglobal teleconnection triggered by spring land thermal anomalies over West Asia and its possible impacts on early summer climate over North China. J Clim 34:5999–6021. https://doi.org/10.1175/JCLI-D-20-0911.1

Yang K, Zhang J (2016) Spatiotemporal characteristics of soil temperature memory in China from observation. Theor Appl Climatol 126(3–4):739–749. https://doi.org/10.1007/s00704-015-1613-9

Yoon J-H, Leung LR (2015) Assessing the relative influence of surface soil moisture and ENSO SST on precipitation predictability over the contiguous United States. Geophys Res Lett 42:5005–5013. https://doi.org/10.1002/2015GL064139

Zhang H, Yuan N, Ma Z, Huang Y (2021) Understanding the soil temperature variability at different depths: effects of surface air temperature, snow cover, and the soil memory. Adv Atmos Sci 38(3):493–503. https://doi.org/10.1007/s00376-020-0074-y

Zhan Y, Lin Z (2011) The relationship between June precipitation over mid-lower reaches of the Yangtze River basin and spring soil moisture over the East Asian monsoon region. Acta Meteorol Sin 25(3):355–363. https://doi.org/10.1007/s13351-011-0310-6

Zhang R, Zuo Z (2011) Impact of spring soil moisture on surface energy balance and summer monsoon circulation over East Asia and precipitation in East China. J Climate 24(13):3309–3322. https://doi.org/10.1175/2011JCLI4084.1

Zhao CY, Chen HS, Sun SL (2018) Evaluating the capabilities of soil enthalpy, soil moisture and soil temperature in predicting seasonal precipitation. Adv Atmos Sci 35(4):445–456. https://doi.org/10.1007/s00376-017-7006-5

Zhong S, Yang T, Qian Y, Zhu J, Wu F (2018) Temporal and spatial variations of soil moisture-Precipitation feedback in East China during the East Asian summer monsoon period: a sensitivity study. Atmos Res 213:163–172. https://doi.org/10.1016/j.atmosres.2018.05.014

Zhou J, Zuo Z, Rong X, Wen J (2020) Role of May surface temperature over eastern China in East Asian summer monsoon circulation and precipitation. Int J Climatol 40(15):6396–6409. https://doi.org/10.1002/joc.6588

Terms and Conditions

Springer Nature journal content, brought to you courtesy of Springer Nature Customer Service Center GmbH (“Springer Nature”).
Springer Nature supports a reasonable amount of sharing of research papers by authors, subscribers and authorised users (“Users”), for small-scale personal, non-commercial use provided that all copyright, trade and service marks and other proprietary notices are maintained. By accessing, sharing, receiving or otherwise using the Springer Nature journal content you agree to these terms of use (“Terms”). For these purposes, Springer Nature considers academic use (by researchers and students) to be non-commercial.
These Terms are supplementary and will apply in addition to any applicable website terms and conditions, a relevant site licence or a personal subscription. These Terms will prevail over any conflict or ambiguity with regards to the relevant terms, a site licence or a personal subscription (to the extent of the conflict or ambiguity only). For Creative Commons-licensed articles, the terms of the Creative Commons license used will apply.
We collect and use personal data to provide access to the Springer Nature journal content. We may also use these personal data internally within ResearchGate and Springer Nature and as agreed share it, in an anonymised way, for purposes of tracking, analysis and reporting. We will not otherwise disclose your personal data outside the ResearchGate or the Springer Nature group of companies unless we have your permission as detailed in the Privacy Policy.
While Users may use the Springer Nature journal content for small scale, personal non-commercial use, it is important to note that Users may not:

1. use such content for the purpose of providing other users with access on a regular or large scale basis or as a means to circumvent access control;
2. use such content where to do so would be considered a criminal or statutory offence in any jurisdiction, or gives rise to civil liability, or is otherwise unlawful;
3. falsely or misleadingly imply or suggest endorsement, approval , sponsorship, or association unless explicitly agreed to by Springer Nature in writing;
4. use bots or other automated methods to access the content or redirect messages
5. override any security feature or exclusionary protocol; or
6. share the content in order to create substitute for Springer Nature products or services or a systematic database of Springer Nature journal content.

In line with the restriction against commercial use, Springer Nature does not permit the creation of a product or service that creates revenue, royalties, rent or income from our content or its inclusion as part of a paid for service or for other commercial gain. Springer Nature journal content cannot be used for inter-library loans and librarians may not upload Springer Nature journal content on a large scale into their, or any other, institutional repository.
These terms of use are reviewed regularly and may be amended at any time. Springer Nature is not obligated to publish any information or content on this website and may remove it or features or functionality at our sole discretion, at any time with or without notice. Springer Nature may revoke this licence to you at any time and remove access to any copies of the Springer Nature journal content which have been saved.
To the fullest extent permitted by law, Springer Nature makes no warranties, representations or guarantees to Users, either express or implied with respect to the Springer nature journal content and all parties disclaim and waive any implied warranties or warranties imposed by law, including merchantability or fitness for any particular purpose.
Please note that these rights do not automatically extend to content, data or other material published by Springer Nature that may be licensed from third parties.
If you would like to use or distribute our Springer Nature journal content to a wider audience or on a regular basis or in any other manner not expressly permitted by these Terms, please contact Springer Nature at

onlineservice@springernature.com